Title

Inhibition of Escherichia coli CTP Synthetase by NADH and Other Nicotinamides and Their Mutual Interactions with CTP and GTP

Journal

Biochemistry, 55(39)

ISSN

0006-2960

Authors

Habrian, Chris
Chandrasekhara, Adithi
Shahrvini, Bita
et al.

Publication Date

2016-10-04

DOI

10.1021/acs.biochem.6b00383

Peer reviewed

BIOCHEMISTRY
including biophysical chemistry & molecular biology

Article

pubs.acs.org/biochemistry

Inhibition of *Escherichia coli* CTP Synthetase by NADH and Other Nicotinamides and Their Mutual Interactions with CTP and GTP

Chris Habrian,[†,‡] Adithi Chandrasekhara,[†,§] Bita Shahrvini,[†] Brian Hua,[†,∥] Jason Lee,[†,⊥,○] Roger Jesinghaus,[†] Rachael Barry,[#,▽] Zemer Gitai,[#] Justin Kollman,[¶] and Enoch P. Baldwin*[,†]

[†]Department of Molecular and Cellular Biology, University of California, Davis, Davis, California 95616, United States
[‡]Biophysics Graduate Program, University of California, Berkeley, Berkeley, California 94720, United States
[§]Process Development Rotation Program, Genentech Inc., 1 DNA Way, South San Francisco, California 94080, United States
[∥]Department of Biology, Massachusetts Institute of Technology, Cambridge, Massachusetts 02139, United States
[⊥]Drexel University College of Medicine, Philadelphia, Pennsylvania 19129, United States
[○]Kaiser Permanente, Sacramento, California 95823, United States
[#]Department of Molecular Biology, Princeton University, Princeton, New Jersey 08544, United States
[▽]Department of Cellular and Molecular Medicine, University of California, San Diego, La Jolla, California 92903, United States
[¶]Department of Biochemistry, University of Washington, Seattle, Washington 98195, United States

Supporting Information

ABSTRACT: CTP synthetases catalyze the last step of pyrimidine biosynthesis and provide the sole *de novo* source of cytosine-containing nucleotides. As a central regulatory hub, they are regulated by ribonucleotide and enzyme concentration through ATP and UTP substrate availability, CTP product inhibition, GTP allosteric modification, and quaternary structural changes including the formation of CTP-inhibited linear polymers (filaments). Here, we demonstrate that nicotinamide redox cofactors are moderate inhibitors of *Escherichia coli* CTP synthetase (*Ec*CTPS). NADH and NADPH are the most potent, and the primary inhibitory determinant is the reduced nicotinamide ring. Although nicotinamide inhibition is noncompetitive with substrates, it apparently enhances CTP product feedback inhibition and GTP allosteric regulation. Further, CTP and GTP also enhance each other's effects, consistent with the idea that NADH, CTP, and GTP interact with a common intermediate enzyme state. A filament-blocking mutation that reduces CTP inhibitory effects also reduced inhibition by GTP but not NADH. Protein-concentration effects on GTP inhibition suggest that, like CTP, GTP preferentially binds to the filament. All three compounds display nearly linear dose-dependent inhibition, indicating a complex pattern of cooperative interactions between binding sites. The apparent synergy between inhibitors, in consideration with physiological nucleotide concentrations, points to metabolically relevant inhibition by nicotinamides, and implicates cellular redox state as a regulator of pyrimidine biosynthesis.

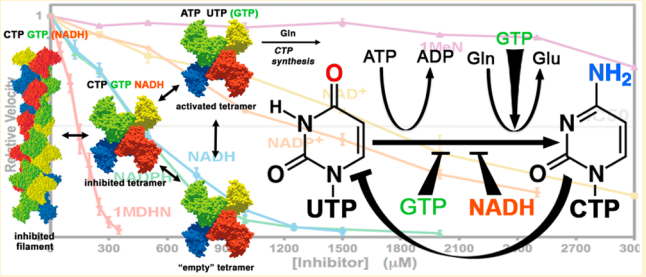

CTP synthetases (CTPSs) are ubiquitous enzymes that produce CTP by amination of UTP[1] (reviewed in ref 2). CTP concentrations are the lowest of the four ribonucleotides in many cells.[3−5] Catalyzing the last step of the pyrimidine biosynthetic pathway and as the only *de novo* source of cytosine nucleotides, CTPSs are critical regulatory hubs with a number of inputs that modulate their activity including ribonucleotide concentrations and phosphorylation.[2,6−10] CTPSs have been suggested as drug targets for cancer, sleeping sickness, and recently, *Mycobacterium tuberculosis* infection.[11−13]

Structural analyses of CTPSs depict an active tetramer composed of two-domain monomers (Figure 1;[2,7,14,15] Welin et al., unpublished, PDB 2VKT, 2W7T). ATP hydrolysis drives this unfavorable reaction by phosphorylating the unreactive UTP O4 atom, and the resulting phosphate is displaced by ammonia derived from glutamine hydrolysis.[16,17] The N-terminal kinase-like amidoligase domain promotes UTP phosphorylation and ammonia transfer reactions, while the C-terminal glutamine amidotransferase domain produces ammonia and coordinates its delivery to the amidoligase active site.

The structural mechanisms of CTPS regulation are only partially understood (Figure 1). All four nucleotides contribute activating or inhibiting inputs. Active tetramer assembly from inactive dimers is promoted by ATP and UTP substrates,[18−22] which bind at an interfacial active site formed by the N-terminal amidoligase domains.[2,7,23] Feedback inhibition is effected by the

Received: April 21, 2016
Revised: August 13, 2016
Published: August 29, 2016

DOI: 10.1021/acs.biochem.6b00383
Biochemistry 2016, 55, 5554−5565

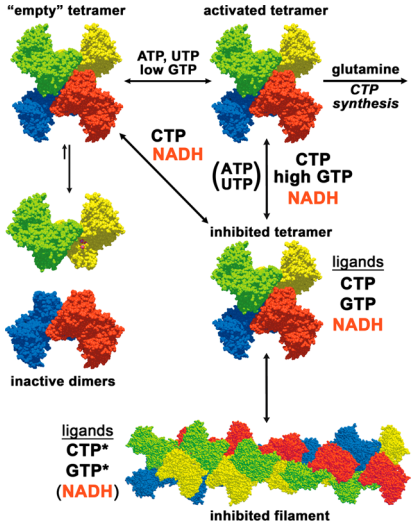

Figure 1. Nucleotide regulation of *Ec*CTPS. *Ec*CTPS is in a dimer−tetramer equilibrium favoring the tetramer in the presence of nucleotides ATP and UTP, since their binding sites are completed upon tetramerization (see refs 2 and 23). GTP (<250 μM) activates glutamine hydrolysis. Product feedback inhibitor CTP binds the tetramer, competitively preventing UTP binding. CTP-bound tetramers are also in equilibrium with an inhibited filament (see ref 31). It is unknown whether *Ec*CTPS dimers bind GTP. Mutual enhancements of each other's inhibitory potencies by CTP, NADH, and GTP and the lack of competition of GTP and NADH with ATP and UTP substrates suggest that they preferentially bind an inhibited tetramer conformation distinct from the "active" one. CTP and NADH can bind this conformation in the absence of other ligands. Responses to a filament-disrupting mutation suggest that CTP and GTP also preferentially interact with the filament (indicated by an asterisk) while NADH does not.

product CTP, which competes with UTP by binding at a distinct but overlapping site.[23] Allosteric regulator GTP is required for efficient CTP synthesis but also can inhibit it; low concentrations (0−200 μM) activate glutamine hydrolysis up to 50-fold, while higher concentrations ($IC_{50} \approx 500$ μM) inhibit CTP synthesis without affecting glutamine hydrolysis.[10] However, its binding sites are still speculative.[2] In many eukaryotes, two independent CTPS isoforms are further regulated by multiple protein phosphorylations.[6,8,9,24−26] More recently, bacterial, human, yeast, and *Drosophila* CTPSs were demonstrated to dynamically aggregate into micrometer-scale linear filaments.[27−30] Barry et al. demonstrated that *Escherichia coli* filaments are a regulatory assembly that is induced by CTP binding.[31] They also determined the filament cryoEM structure, which revealed a superhelix of tetramers. Analyses of human, *Drosophila*, and yeast enzymes suggest that different factors might control eukaryotic filament formation and structure.[32−34]

While ribonucleotide influences on CTPS activity are relatively well characterized, there has been no evidence for its regulation by other metabolites. Serendipitously, we discovered that the redox cofactor NADH inhibits *E. coli* CTP synthetase (*Ec*CTPS). Here, we describe inhibition by nicotinamides and their interactions with other known *Ec*CTPS regulators. Although by themselves nicotinamides are moderate inhibitors, their apparent synergy with other natural inhibitors suggests that their effects on *Ec*CTPS may be physiologically relevant.

MATERIALS AND METHODS

Enzyme Production. *Ec*CTPS was expressed as an N- or C-terminal His_6 fusion protein. The *Ec*CTPS reading frame was amplified from *E. coli* K-12 and ligated into pET28b, fused in frame to the N-terminal His6 tag sequence at the *Nde*I site.[23] The C-terminal His-tagged protein was created by replacing the N-terminal region *Xba*I−*Nde*I fragment with that of pET41 to yield the native N-terminus, while deletion mutagenesis fused the C-terminal lysine residue to a His6 tag via a Val−Glu linker.

*Ec*CTPS enzymes were overexpressed and purified using metal chelate chromatography. Proteins were produced in BL21(DE3)* cells, which express rare tRNAs (Life Technologies), enhancing yields 1.5−2-fold over BL21(DE3). One liter of culture was inoculated with a single fresh colony and grown on LB broth at 37 °C until A_{600nm} reached 0.6−0.8 and then induced with 100 μM IPTG. After 3−5 h growth, cells were centrifuged (2000*g*, 10 min, 4 °C), and the pellets were stored at −80 °C. Cell pellets were thawed on ice, resuspended in lysis/wash buffer (20 mM Tris-Cl, 5 mM imidazole, 500 mM NaCl, pH 7.9) containing 1 mM PMSF, and lysed using a microfluidizer. The cleared lysates (15 000*g*, 45 min, 4 °C) were loaded onto 3−5 mL beds of Ni-NTA resin equilibrated with lysis/wash buffer. The columns were washed with 200 mL of lysis/wash buffer, followed by 200 mL of lysis/wash buffer containing 2 M NaCl, and then again with 200 mL of lysis/wash. The proteins were eluted with minimal elution buffer (20 mM Tris-Cl, 500 mM imidazole, 500 mM NaCl, pH 7.9), and immediately dialyzed against 20 mM Tris-Cl, 10 mM EDTA, 500 mM NaCl, pH 8.1 for 4 h, followed by overnight dialysis against 20 mM Tris-Cl, 0.1 mM EDTA, 500 mM NaCl, 2 mM DTT, pH 8.1. The dialyzed eluates were concentrated using Amicon Y-100 spin concentrators to 10−15 A_{280} units/mL, then flash-frozen in 50 μL aliquots and stored at −80 °C. Typical recoveries were 20−30 mg of purified *Ec*CTPS per liter of cell culture. For assays, storage tubes were rapidly thawed under running cold water, immediately mixed, and stored at 4 °C. Maximum activity was achieved within 12 h after thawing and diminished with extended storage at 4 °C. Freezing and storage in 500 mM NaCl-containing buffer extended the half-life of thawed enzyme to more than 6 weeks, compared to about 3 weeks using a buffer with no added salt.

Quantification of Protein, Nucleotide, and Nicotinamides. Enzyme concentrations were determined from the 280 nm absorbance. To make our data comparable to previous work, we used the historical extinction coefficient $0.89A_{280}$ mg^{-1}-mL^{-1} (5.5×10^3 M^{-1}).[35] It should be noted that the EXPASY PROTPARAM calculator (http://web.expasy.org/protparam/) yields values of $0.67A_{280}$ mg^{-1}-mL^{-1} and 4.0×10^3 M^{-1}, which would result in a 1.33-fold higher protein concentrations than are indicated.

Solid nucleotides were obtained from Sigma-Aldrich unless otherwise noted. The structures of the nicotinamides used in this study are depicted in Figure 2. Solutions were prepared by dissolving solids in equimolar Na-HEPES pH 8.0 at twice the desired final concentration: 100 mM for ATP (no. A3377), UTP (no. U6750 or no. U6875), CTP (no. C1506), NADH (no. N6505), NADPH (no. N7505), NAD^+ (no. N0632), and $NADP^+$ (no. N0505); 0.02 mM for GTP (no. G8877); 100 mM for 1-methyl dihydronicotinamide (1MDHN, Santa Cruz Biotechnology, no. sc-213351); and 250 mM for 1-methylnicotinamide (1MeN, Santa Cruz Biotechnology, no. sc-237583). Monitored with pH paper, the pH was adjusted to

DOI: 10.1021/acs.biochem.6b00383
Biochemistry 2016, 55, 5554−5565

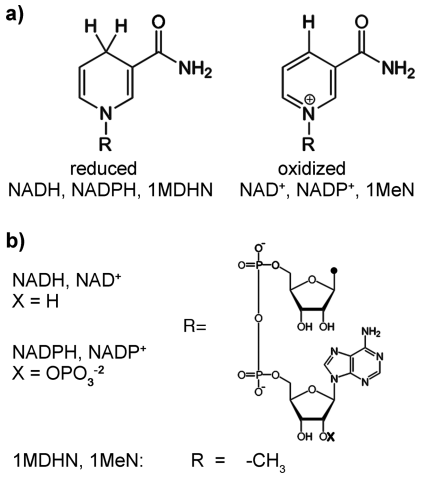

Figure 2. Structures of nicotinamide compounds used in this study. (a) Structural differences between reduced and oxidized nicotinamide rings. Oxidized forms are aromatic, charged, and planar, while reduced forms are neutral and in a "boat" conformation. (b) Structural differences between the different R groups of the nicotinamides. Phosphorylation occurs on the 2′-OH of the adenylate portion of NAD^+/NADH (−OX) to give $NADP^+$/NADH.

7.5−8.0 using 1 M NaOH. Nucleotide concentrations were determined from UV absorbance using the appropriate extinction coefficient (ATP, ε(259 nm) = 1.54 × 10^4 M^{-1}; UTP, ε(262 nm) = 1.00 × 10^4 M^{-1}; GTP, ε(253 nm) = 1.37 × 10^4 M^{-1}; CTP, ε(271 nm) = 9.0 × 10^3 M^{-1}; NADH/NADPH, ε(339 nm) = 6.22 × 10^3 M^{-1}; NAD^+/$NADP^+$, ε(259 nm) = 1.7 × 10^4 M^{-1}; 1MDHN, ε(360 nm) = 7.06 × 10^3 M^{-1};[36] 1MeN, ε(265 nm) = 3.94 × 10^3 M^{-1}).[37] The mixtures were diluted to their final storage volumes with water and requantified by UV absorbance. Stocks were apportioned into 50−150 uL aliquots in screw-capped tubes prior to freezing at −80 °C. Concentrations of further dilutions were redetermined prior to use. Solutions of 1MDHN oxidized rapidly at 4 °C, and aliquots were only allowed to stand for less than 2 h before use. Glutamine stocks (Sigma/Aldrich no. G3126, 100 mM in 1 mL aliquots) were treated similarly except that no pH adjustment was necessary and concentrations were solely based on weight.

CTP Synthesis Assay. Assays were carried out using an HP-6853 spectrophotometer outfitted with a water-jacketed 8-cell cuvette holder. The cuvettes were pre-equilibrated at 37 °C (liquid temperature in cuvette). Absorbance at 291 nm versus time data were acquired using the UV−visible Chemstation software package in "Kinetics" mode. Sampling times were 0.5−8 s depending on the duration of the experiment (100−500 s).

Reaction buffer contained 60 mM Na-HEPES, pH 8.0, 10 mM $MgCl_2$, 0.5 mM EGTA, and 2 mM Na-azide. Standard saturating substrate concentrations were 600 μM UTP, 1.5 mM ATP ,and 10 mM glutamine. The $S_{0.5}$ values are given in Table 1. Unless otherwise stated, 200 μM GTP and 200 nM *Ec*CTPS were used. Both N-terminal and C-terminal His-tagged enzymes yielded indistinguishable kinetic values and protein-concentration dependencies on specific activity. The majority of the inhibition data reported here were obtained using the N-terminal His-tagged form.

The reaction procedure is illustrated in Figure 3a. For each reaction, three tubes were prepared: "A" tubes contained nucleotides, inhibitors, and reaction buffer, "B" tubes contained 2 μM *Ec*CTPS in reaction buffer, and "C" tubes contained 100 mM glutamine. Component concentrations were adjusted to

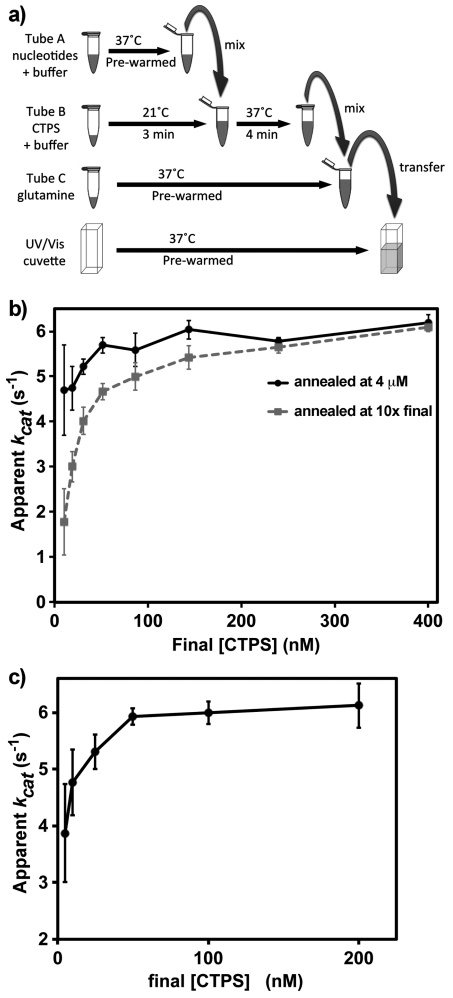

Figure 3. *In vitro* *Ec*CTPS reactions. (a) Scheme for performing *Ec*CTPS reactions. *Ec*CTPS enzyme (2−40 μM) was annealed for 3 min at 21 °C in reaction buffer then mixed with prewarmed nucleotide substrates and effectors and incubated for an additional 4 min at 37 °C. To initiate the synthesis reaction, the enzyme−nucleotide solutions were mixed with 10-fold concentrated 37 °C glutamine solution and immediately transferred to 37 °C cuvettes to measure the change in UV absorbance at 291 nm. (b) Concentration dependence of the annealing reaction on specific activity (apparent k_{cat}). Different amounts of *Ec*CTPS were annealed at either 4 μM (black circles) or at 10-fold final concentration (100−4000 nM, gray squares) *Ec*CTPS prior to dilution to 10−400 nM into nucleotides and glutamine as described in panel a and Materials and Methods. Note that the apparent k_{cat} values for the two curves converge between 2 and 2.4 μM. (c) Dependence of apparent k_{cat} values on final [*Ec*CTPS] in the reaction. In a separate experiment from panel b, 4 μM *Ec*CTPS was preincubated at 21 °C, then diluted to the final concentrations indicated on the horizontal axis (5−200 nM) upon addition of nucleotides and glutamine as described in panel a and Materials and Methods. Under these conditions, k_{cat} increases approximately 5−9% going from 100 to 500 nM final *Ec*CTPS (Figure S8).

achieve the desired final levels when the contents of all three tubes are combined. A and C tubes were pre-equilibrated at 37 °C. At time = 0, B tubes, stored on ice, were transferred to a room temperature water bath (21−22 °C) and incubated for 3 min ("annealing"). The contents of tube A were then added, and the mixture was further incubated at 37 °C for 4 min. CTP synthesis was initiated by transferring the entire contents to

DOI: 10.1021/acs.biochem.6b00383
Biochemistry 2016, 55, 5554−5565

tube C, mixing, and then immediately transferring the mixture to a prewarmed cuvette.

In protein-dependent experiments in which high (>2 μM) protein concentrations were used (Figure 7c), *Ec*CTPS was annealed at 40 μM, and the reactions were carried out as previously described.[31] At the highest final EcCTP concentration used (8 μM, Figure 7c), the NaCl contribution from enzyme stocks did not exceed 20 mM, which has a negligible effect on rate (Figure S1). The maximum additional sodium ion contributions from triphosphates and nicotinamides ranged 11−18.5 mM. This amount represents a significant increase above the reaction buffer contribution (46 mM). However, based on the effects of 0.1 M NaCl (Figure S1) or 0.1 M NaOAc (Figure S6) on apparent k_{cat}, the velocity reduction due to 20 mM additional sodium ion is 4.4−6% (0.22−0.30%/mM Na^+). The sodium ion concentration differences in comparisons between inhibitor titrations in the absence or presence of another inhibitor were 1−1.9 mM.

*Ec*CTPS requires at least 2 mM free magnesium ion for maximal activity.[38] The maximum triphosphate concentrations used here were 2.3−3.9 mM, allowing for greater than 6 mM minimum free magnesium ion.

Data Analysis. CTP production velocities were calculated using the extinction coefficient difference between UTP and CTP at 291 nm, 1338 M^{-1}.[39] The delay between glutamine mixing and the first spectrophotometric data point was 5−10 s. Linear rates persisted for at least 10−20 s unless substrates were limiting. Initial rates were extracted from the earliest linear regions (6−20 data points) of the A_{291} versus time data using linear regression.

Descriptive substrate kinetic parameters were obtained by nonlinear fitting of velocity data to the Hill equation

$$\frac{v}{V_{max}} = \frac{[S]^{n_H}}{[S_{0.5}]^{n_H} + [S]^{n_H}}$$

using the Solver Add-in function in Excel to minimize the value of the sum of the squared differences between calculated and observed rates. Substrate titrations yielded linear Hill plots over the concentrations ranges used (ATP, 35−1500 μM; UTP, 15−600 μM; glutamine 100−5000 μM). All inhibition data yielded nonlinear Hill plots, apparently biphasic (for CTP, see Figure 4a) so we reported descriptive IC_{50} values, which were determined by linear extrapolation between the two data points that straddled the 50% activity value (Tables 2 and 3). Mean values and standard deviations for all kinetic constants were calculated from individual experimental values using Excel. In an attempt to understand the Hill plot curvature and the nature of inhibitor binding cooperativity, we fit NADH and CTP *v* vs [I] inhibition data to a generalized sequential binding model for a tetramer:[40]

$$\frac{v}{V_o} = 1 - \frac{\frac{[I]}{K_1} + \frac{3[I]^2}{K_1K_2} + \frac{3[I]^3}{K_1K_2K_3} + \frac{[I]^4}{K_1K_2K_3K_4}}{1 + \frac{4[I]}{K_1} + \frac{6[I]^2}{K_1K_2} + \frac{4[I]^3}{K_1K_2K_3} + \frac{[I]^4}{K_1K_2K_3K_4}}$$

where each K_n corresponds to the dissociation constant between binding $n-1$ and n inhibitors. The model is highly simplified, and low data/parameter ratios limited fitting accuracy. Boundary restraints were applied to K_1 and the ratios K_2/K_1, K_3/K_2 and K_4/K_3 (>0, 0.03−1000, 0.03−1000, 0.00001−30, respectively). For some data sets, one additional low inhibitor concentration value between 0 and the first measured concentration point was added due to lack of data coverage, estimated from other experiments outside the fit data sets. These points were required to prevent K_1 from becoming unrealistically small, K_2 from becoming concomitantly unrealistically large, and the calculated binding curve from unusual developing extreme downward concavity at the low concentration range during fitting cycles. Even without these points, the patterns of apparent cooperativity were consistent (see Discussion).

Initial values of K_1, K_2, K_3, and K_4 were set to the experimental IC_{50} values. Although the fitted values were sensitive to initial estimates, the trends over a 10-fold range of initial values were robust and suggested complex cooperativity patterns (see Discussion).

Descriptive values EC_{50} and IC_{50} were also reported for the activation and inhibition portions of the GTP dose−response curves and were calculated analogously to the $S_{0.5}$ values (Tables 2 and 3). For comparison purposes, we also fit the data to a two-site activation/inhibition model from Bearne and coworkers,[10]

$$\text{apparent}k_{cat} = \frac{\frac{k_{act}[GTP]}{K_A}}{\left(1 + \frac{[GTP]}{K_A} + \left(\frac{[GTP]}{K_i}\right)^n\right)}$$

with the assumptions that *Ec*CTPS is inactive in the absence of GTP and is fully inhibited by it. GTP parameters and data are reported in the legend for Figure 6.

RESULTS

Activity Assay Optimization. *Ec*CTPS kinetic constants were reported previously,[16,19,22,35,39,41,42] but the collective results did not agree well. Our own initial attempts also yielded inconsistent values. We traced these problems to enzyme storage, determination of nucleotide concentrations, assay enzyme concentrations, and preincubation conditions. Our present assay procedure incorporates additional features that greatly improve reproducibility: careful spectrophotometric determination of nucleotide concentrations, enzyme storage in high salt and room-temperature preincubation ("annealing") at high enzyme concentration prior to exposure to substrates (See Materials and Methods, Figure 3a). At 4 °C, *Ec*CTPS reportedly dissociates into monomers but reforms dimers when shifted to higher temperature.[19,43] The annealing procedure, which is aimed at maximizing dimer reassembly, improved assay reproducibility and increased the specific activity by 20−40% (Figure S2). The protein concentration during annealing was also critical, with maximum specific activity achieved between 2 and 4 μM *Ec*CTPS. Annealing at a fixed high concentration prior to enzyme dilution into substrate/buffer solution lead to a smaller apparent k_{cat} dependence on final enzyme concentration compared to annealing at 10-fold final concentrations (annealing concentrations of 50 nM to 2 μM, compare solid black and dashed gray lines, Figure 3b). Even when annealing was performed at 4 μM enzyme, the specific activity increased 50% between 5 and 50 nM final *Ec*CTPS (Figure 3c), which we attribute to the CTPS dimer−tetramer equilibrium favoring the active tetramer at higher CTPS concentrations. At assay concentrations higher than 2 μM, the specific activity decreased due to inhibitory filament formation.[31] The apparent k_{cat} values, typically 5.5−6.5 s^{-1}, ranging up to 8 s^{-1}, at 200 nM enzyme, are comparable to those reported elsewhere.[16,19,22,42]

Our kinetic constants were robust over a number of individual experimentalists and enzyme preparations. For the

DOI: 10.1021/acs.biochem.6b00383
Biochemistry 2016, 55, 5554−5565

data reported here, baseline characterizations of UTP, ATP, CTP, and GTP concentration dependences, data from two or three individual experimentalists and two to four distinct enzyme preparations were utilized. Subsequently, seven additional experimentalists have obtained average $S_{0.5}$, EC_{50}, or IC_{50} values within 1 SD of those reported here (data not shown). The k_{cat} values vary the most (ranging 40−60%), in part because of different ages of the thawed enzyme. *N*-values are given in Tables 1 and 2 as well as the figure legends.

Our ATP and UTP $S_{0.5}$ values, 60 and 130 μM, respectively, at saturating concentrations of other substrates (Table 1 and Figure S3), agreed well with some reported values[16] but differed from others.[19,22,39,44] As previously observed,[19] the $S_{0.5}$ values of ATP and UTP are interdependent (Table 1). At subsaturating ATP concentration (150 μM), the $S_{0.5}$ of UTP increased to 200 μM, while at 60 μM UTP, the ATP $S_{0.5}$ value increased to 330 μM. Interestingly, we found that lowering the GTP concentration from the optimal (200 μM) to its EC_{50} (50 μM) also reduced the ATP $S_{0.5}$ value to 81 ± 5 μM (n = 5). However, at 500 μM GTP, the ATP $S_{0.5}$ value was similar to that measured at 200 μM GTP (155 ± 25 μM, n = 5).

Protein concentration did not significantly affect the UTP $S_{0.5}$ value at saturating ATP, between 10 and 2000 nM *Ec*CTPS, and had no significant effect on the ATP $S_{0.5}$ value at saturating UTP, from 50 to 400 nM *Ec*CTPS (Table 1, footnotes b and c, and Figure S3). This result is curious since the tetramerization equilibrium is thought to be coupled to UTP binding[18,19,22] and the reduced k_{cat} at low *Ec*CTPS concentrations suggested incomplete tetramer formation (Figure 3c). Therefore, in addition to tetramer formation, the UTP−ATP interdependence may be exerted via on-enzyme site−site interactions.

The GTP concentration dependence of specific activity resembled that previously measured[10] and when fit to the same two-site activation/inhibition model yielded parameter values that agreed within a factor of 2 (Table 1, footnote h).

From these data, we codified "standard assay conditions" of 200 nM final enzyme annealed at 2 μM with saturating substrates 600 μM UTP, 1500 μM ATP, and 10 mM glutamine and 200 μM GTP effector.

Under standard conditions, the IC_{50} of feedback inhibitor CTP is ∼370 μM, whereas at 50 μM UTP (near the UTP $S_{0.5}$ value), the CTP IC_{50} is 160 μM. These values are comparable to those measured under similar conditions.[39,44] Thus, at 50 μM UTP, the CTP IC_{50} is 2.5-fold higher than the UTP concentration, while at saturating UTP (600 μM), the IC_{50} is 1.6-fold lower (Table 1). This increase in relative inhibitory potency when the competitive substrate concentration increases suggests cooperativity between UTP and CTP binding and underscores the complexity of intersite interactions in CTPSs. In fact, the dose-dependence curve for CTP inhibition is atypical (Figure 4a) in that it was nearly linear up to 85% inhibition at 750 μM CTP (R = 0.993) and yielded an apparently biphasic Hill plot (See Materials and Methods and Figure 4a, inset). This behavior has not been previously described and suggests that cooperative interactions between CTP binding sites in the tetramer follow a complex pattern (see Discussion). This behavior was also observed for nicotinamide and GTP inhibition.

Table 1. Kinetic Constants for *Ec*CTPS at 37°C[a]

limiting substrate	condition[a]	$S_{0.5}$ (μM)	Hill coeff, n_H
UTP		59 ± 15	1.4 ± 0.3 (23)[b]
	150 μM ATP	200 ± 40	1.8 ± 0.1 (6)
ATP		130 ± 10	1.7 ± 0.2 (18)[c]
	60 μM UTP	310 ± 20	1.9 ± 0.4 (5)
glutamine[d]		360 ± 20[e]	1.1 ± 0.1 (11)
effector	**condition[a]**	**IC_{50}/EC_{50} (μM)**	
CTP		IC_{50}	370 ± 60[f] (6)
	50 μM UTP 100 nM *Ec*CTPS	IC_{50}	160 ± 10[g] (4)
GTP[h]		EC_{50}	38 ± 3 (4)
		IC_{50}	540 ± 60

[a]Unless noted, substrates were present at saturation with optimal GTP. ([UTP] = 600 μM, [ATP] = 1500 μM, [GTP] = 200 μM, [glutamine] = 10 mM). $S_{0.5}$ and n_H values were determined by fitting data to the Hill function. IC_{50} values were estimated by linear extrapolation of data points straddling 50% inhibition values (see Materials and Methods). The number of experiments used for each determination is given in parentheses. [b]The $S_{0.5}$ and n_H values did not significantly vary from 10 to 2000 nM enzyme (at 100 nM, $S_{0.5}$ = 57 ± 8, n_H = 1.3 ± 0.2, from seven experiments). [c]The $S_{0.5}$ and n_H values did not significantly vary from 50 to 400 nM enzyme (at 100 nM, $S_{0.5}$ = 126 ± 13, n_H = 1.7 ± 0.3, from six experiments). [d]These values were determined at 100 nM enzyme and include four values determined in the presence of 500 μM NADH, which had no discernible effect. [e]Lineweaver−Burke analysis gave 411 ± 44 μM as the K_m value. Bearne and Iyengar reported a K_m of 320 μM using HPLC.[58] [f]The limiting slopes of the biphasic Hill plots were −1.22 ± 0.3 and −4.8 ± 1.9, at the low and high concentration ranges, respectively. [g]The limiting slopes of the biphasic Hill plots were −0.6 ± 0.2 and −1.9 ± 0.3, at the low and high concentration ranges, respectively. [h]GTP EC_{50} and IC_{50} values were estimated by linear extrapolation of data points straddling 50% activation and inhibition values, respectively. Nonlinear Hill plots yielded limiting slopes of 1.8 ± 0.2 and −4.6 ± 0.3, at the low and high concentration ranges, respectively. Fitting the data from individual experiments to a two-site model,[10] where n_{act} = 1, gave the following averaged parameters: k_{act} = 10.0 ± 0.6 s^{-1}, K_A = 57 ± 7 μM, K_i = 308 ± 24 μM, and n_{inh} = 5.0 ± 0.4. Previously reported values were, respectively, 10.3, 23, 190, and 3.8.[10]

EcCTPS Is Inhibited by Nicotinamides. *Ec*CTPS is inhibited by nicotinamide-containing compounds. Dose-dependent inhibition data for six nicotinamides, determined under standard assay conditions, is shown in Figure 4b and Table 2.

NADH inhibits CTP synthesis activity with an IC_{50} of 470 μM, with greater than 95% inhibition at 1250 μM. Inhibition potency was independent of enzyme concentration from 50 to 400 nM (Figure S4). Like CTP, the dose dependence was complex, being nearly linear from 0 to 750 μM, and yielded nonlinear Hill plots. Potent inhibition required the reduced cofactor. The oxidized NAD^+ cofactor inhibited ∼3-fold less effectively (IC_{50} = 1700 μM). NADPH had similar inhibitory potency to NADH. Curiously, $NADP^+$ was a somewhat better inhibitor than NAD^+ (IC_{50} = 1280 μM) and concentration dependence for both 2′-phosphorylated cofactors exhibited slightly more curvature.

The reduced nicotinamide ring is a critical recognition element. The NADH analog 1-methyl 1,4-dihydronicotinamide (1MDHN, Figure 2) is more effective than NADH (IC_{50} = 140 μM), whereas the oxidized analog 1-methylnicotinamide (1MeN) was a very poor inhibitor (<25% inhibition at 3000 μM).

The inhibitory properties of NADH/NADPH and NAD^+/$NADP^+$ do not apparently involve critical interaction of the adenine nucleotide portion with the ATP site, since ATP had the same $S_{0.5}$ value in the presence or absence of these cofactors. In agreement with this idea, ADP was a poor

DOI: 10.1021/acs.biochem.6b00383
Biochemistry 2016, 55, 5554−5565

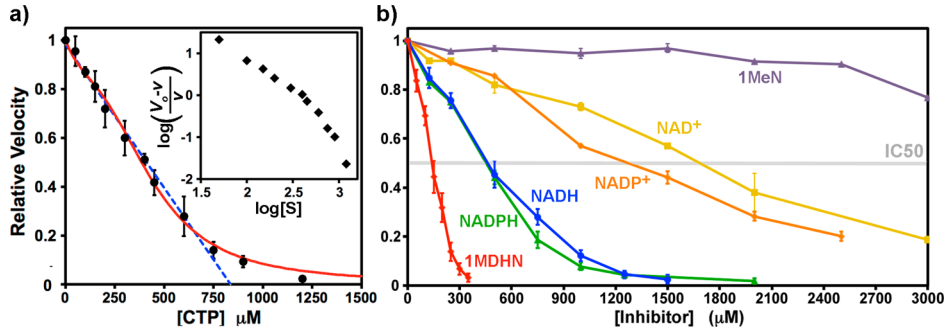

Figure 4. (a) Dose–response curve for CTP inhibition. Data points are indicated (black circles) as the averages of three, six, or nine separate determinations. The error bars indicate ±SD. The dose response is nearly linear up to 750 μM CTP (blue dashed line, $R = 0.993$). The best-fit curve to a four-site sequential binding model is also shown (red curve, see Materials and Methods). The parameters K_1, K_2, K_3, and K_4 were 446, 2120, 1173, and 7.5 μM, respectively. The fit IC_{50} value is 385 μM. A Hill plot is shown in the inset. The limiting slopes at low and high CTP concentrations are −1.5 and −4.0, respectively, and the average slope is −2.0. (b) Dose-dependent *Ec*CTPS inhibition by various reduced and oxidized nicotinamide compounds. Each line is labeled and color-coded for the particular compound (see Figure 2). Reactions were performed under standard conditions (see Materials and Methods), with inhibitors present during the nucleotide preincubation period (see Figure 3). Numeric IC_{50} values are found in Table 2.

Table 2. Inhibition Constants for Nicotinamide *Ec*CTPS Inhibitors[a]

inhibitor	IC_{50},[b] μM	$IC_{50}^{ox}/IC_{50}^{red}$
NADH	470 ± 40 (6)	3.7
NAD^+	1700 ± 70 (2)	
NADPH	450 ± 20 (3)	2.8
$NADP^+$	1280 ± 50 (3)	
1MDHN	140 ± 10 (7)	>28
1MeN	4000(est) (2)	
ADP	4500(est) (2)	

[a]All reactions contained 200 nM *Ec*CTPS, 1.5 mM ATP, 0.6 mM UTP, 0.2 mM GTP, and 10 mM glutamine. [b]IC_{50} values were estimated by linear extrapolation of data points straddling 50% inhibition values. All nicotinamide inhibitors yielded nonlinear Hill plots, with limiting slopes of −0.89 ± 0.16 and −4.0 ± 1.0, at the low and high concentration ranges, respectively. The numbers of independent determinations used in the calculations are given in parentheses.

inhibitor with only 35% inhibition at 3000 μM (est. $IC_{50} \approx 4.5$ mM, Table 2). The v vs [S] curves obtained varying UTP or glutamine were also unaffected by NADH or 1MDHN. Conversely, when titrated in the presence of ATP, UTP, or glutamine substrates at their $S_{0.5}$ values, the NADH dose–response curves were identical to those with saturating substrates (Figure S5). These data demonstrate that nicotinamide inhibition is noncompetitive with ATP, UTP, and glutamine.

NADH, CTP, and GTP Mutually Increase Each Other's Potency. To probe potential on-enzyme interactions between inhibitors, we titrated CTP synthesis reactions with each inhibitor in the presence of the others near their IC_{50} values (Table 3). In the presence of 400 μM CTP, the shape of the NADH dose–response curve became more concave and the apparent NADH inhibition potency increased ∼2.1-fold with an IC_{50} of 220 μM (Figure 5a). Similarly, in the presence of 500 μM NADH, CTP is a 2.3-fold more potent feedback inhibitor (IC_{50} = 160 μM) (Table 3, Figure 5b). Thus, the two apparently increase each other's inhibitory activity in a mutual fashion. Similar behavior was observed with 1MDHN and CTP: 140 μM 1MDHN increased CTP inhibition potency 1.8-fold, and 400 μM CTP increased 1MDHN potency more than 2-fold (Table 3). Although NAD^+ was a weaker inhibitor, at its IC_{50}, CTP efficacy increased similarly as with NADH (Table 3), suggesting that both oxidized and reduced forms inhibit by similar mechanisms.

GTP is an activator at low concentrations ($EC_{50} \approx 38$ μM, maximum activation at ∼200 μM) and an inhibitor at concentrations above 250 μM, with an IC_{50} of 540 μM (Table 1, Figure 6b). As with CTP, NADH inhibition was enhanced by GTP (Figure 6a). NADH inhibitory strength increased with increasing GTP over both activating and inhibiting concentrations. From 50 to 500 μM GTP, the NADH IC_{50} value decreased from 770 to 240 μM. Complementarily, 500 μM NADH altered the GTP concentration dependence, steepening both the activation and inhibition portions of the curve (EC_{50} = 24 μM, IC_{50} = 350 μM) (Figure 6b) and shifting the optimal GTP concentration to approximately 100 μM. At its IC_{50}, 1MDHN had a similar effect on the GTP dose–response of *Ec*CTPS activity as

Table 3. Interactions between NADH, CTP, and GTP[a]

	none[b]	400 μM CTP	500 μM NADH	50 μM GTP	500 μM GTP	140 μM 1MeDHN	1200 μM NAD^+
CTP IC_{50}	370 ± 60		160 ± 40 (4)	620 ± 30 (3)	220 ± 60 (3)	200 ± 20 (3)	160 ± 30 (2)
NADH IC_{50}	470 ± 40	220 ± 90 (4)		770 ± 30 (3)	240 ± 10 (3)		
GTP EC_{50}	38 ± 3	21 ± 2 (4)	24 ± 2 (4)			20 (1)	
GTP IC_{50}	540 ± 60	410 ± 50 (4)	350 ± 40 (4)			330 (1)	
1MDHN IC_{50}	140 ± 10	73 ± 6 (3)					

[a]IC_{50} and EC_{50} values are given in micromolar concentrations. All reactions contained 200 nM *Ec*CTPS, 1.5 mM ATP, 600 μM UTP, 10 mM glutamine, and 200 μM GTP, unless otherwise noted. The number of independent measurements for each experiment is given in parentheses. [b]Values from Tables 1 and 2.

DOI: 10.1021/acs.biochem.6b00383
Biochemistry 2016, 55, 5554–5565

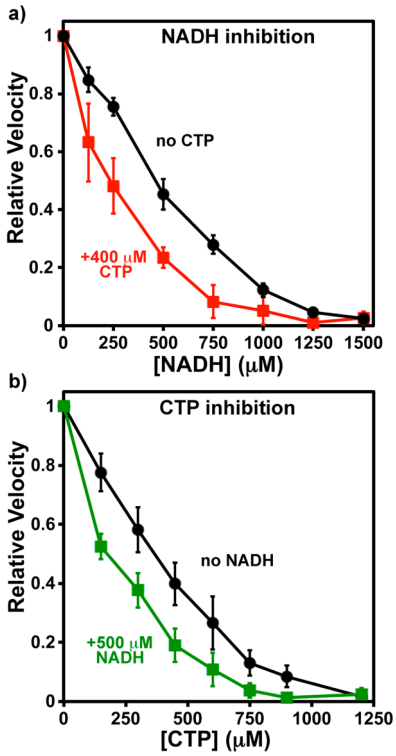

Figure 5. Interactions between NADH and CTP. Error bars indicate the standard deviation of the indicated number of experiments after normalizing to V_0 equal to one. IC_{50} values are given in Table 3. (a) Relative CTP synthesis velocities with 0−1500 μM NADH in the absence (black circles) or presence (red squares) of 400 μM CTP. The average V_0 values were 1.23 ± 0.05 (n = 6) and 0.61 ± 0.05 μM s^{-1} (n = 4), respectively. (b) Relative velocities with 0−1200 μM CTP in the absence (black circles) or presence (green squares) of 500 μM NADH. The average V_0 values were 1.31 ± 0.30 (n = 6) and 0.66 ± 0.01 μM s^{-1} (n = 4), respectively.

NADH (Table 3). Therefore, GTP and NADH also apparently increase each other's activities.

Since NADH amplified the effects of both CTP and GTP, we investigated whether these two inhibitors also act collaboratively. Indeed, the presence of one modifies the concentration dependence of the other. As GTP concentration increased from 50 to 500 μM, the CTP IC_{50} decreased from 620 to 220 μM (Figure 6c). In turn, and similar to NADH, 400 μM CTP shifted the GTP EC_{50} and IC_{50} values to lower concentrations, from 38 μM and 540 μM to 21 μM and 410 μM, respectively (Figure 6d). The data suggest that NADH, CTP, and GTP are mutually synergistic (See Discussion). Plots of $1/IC_{50}$ versus GTP concentration yielded a straight lines with nonzero intercepts at 0 μM GTP corresponding to 1080 and 860 μM for NADH and CTP, respectively (R = 0.995). These results imply that both inhibitors can bind to *Ec*CTPS without GTP, albeit with lower affinity.

Testing the Role of the Inhibited Filament in Inhibitor Interactions. This mutual enhancement of CTP, GTP, and NADH effects suggests that these molecules interact with the same conformation of the enzyme. One possibility was that NADH and GTP stabilize the CTP-bound inhibitory filament described by Barry et al.[31] In that work, we demonstrated that the presence of CTP increased the self-inhibition of the enzyme at high concentrations, presumably by selectively binding the filament conformation over the free tetramer. Likewise, CTP was a more effective inhibitor at high enzyme concentrations that favor filament formation. We also demonstrated that a mutation that compromised filament formation, E277R, also reduced CTP inhibitory potency.

To test the filament role in NADH and GTP inhibition, we compared the activities of wild-type and E277R *Ec*CTPS at different NADH and GTP concentrations. The NADH dose−response showed no significant differences between wild-type and mutant (Figure 7a). For GTP, the E277R dose−response curve was shifted toward higher concentrations, particularly for the inhibitory portion (Figure 7b). Furthermore, at 4 μM *Ec*CTPS, a concentration at which filament formation reduced activity by ∼50%,[31] the dose−response was shifted toward lower concentrations (Figure 7b). Interestingly, *Ec*CTPS self-inhibition from filament formation was magnified by increasing GTP from 50 to 500 μM. (Figure 7c). Taken together, these data suggest that some GTP interactions with *Ec*CTPS, unlike those of NADH, are linked to protein−protein interactions within the inhibitory filament.

DISCUSSION

Central metabolic pathways are commonly regulated by intermediates related to their products or precursors; for example, *Ec*CTPS is inhibited by its product CTP (Figure 1) and activated by ATP and UTP substrates. Metabolites may also regulate multiple pathways through "cross-talk"; for example, GTP allosteric regulation of *Ec*CTPS. "Reporter metabolites" globally communicate cellular metabolite and energy status to the metabolic network, which integrates their inputs to optimize pathway outputs over a wide range of conditions.[45] Indeed, nicotinamides epitomize this role. In bacteria, conserved Rex repressors link carbon and energy metabolism to redox state,[46,47] as reported by NADH/NAD^+ levels and ratio, thereby controlling operons involved in anaerobic respiration, fermentation, and amino acid metabolism. Nicotinamides also modulate some enzyme activities, either directly through substrate availability (oxidases, dehydrogenases, histone deacetylases) or much less commonly through allosteric regulatory interactions[48] (citrate synthase, phosphorylase, phosphoribulokinase, and pyruvate kinase[49−52]). Nicotinamide regulatory targets control both short-term cellular responses, such as metabolic pathway and operon outputs, and long-term ones, like epigenetic modifications. Our data point to pyrimidine biosynthesis as a potential nicotinamide-regulated pathway.

Nicotinamides inhibit *Ec*CTPS with moderate affinities, with reduced forms having higher inhibitory potency than oxidized forms. Inhibition is noncompetitive with substrates but increases the effectiveness of both product inhibitor CTP and allosteric modifier GTP. We further showed that CTP and GTP also amplify each other's potencies. Together, the data suggest that all three molecules inhibit *Ec*CTPS via a common enzyme conformation. The mutual binding enhancements by these metabolites may shift nicotinamide dose−responses into concentration ranges that can contribute to cellular *Ec*CTPS regulation.

The primary inhibitory determinant is the dihydronicotinamide moiety, since the cofactor analog 1MDHN is more potent than the complete cofactor. The dihydronicotiamide ring may provide a framework for discovery of novel *Ec*CTPS inhibitors. Although the affinity is modest, the N1 atom is readily derivatized allowing for the synthesis and evaluation of a number of analogs. Unlike 1MDHN, the oxidized analog 1MeN

DOI: 10.1021/acs.biochem.6b00383
Biochemistry 2016, 55, 5554−5565

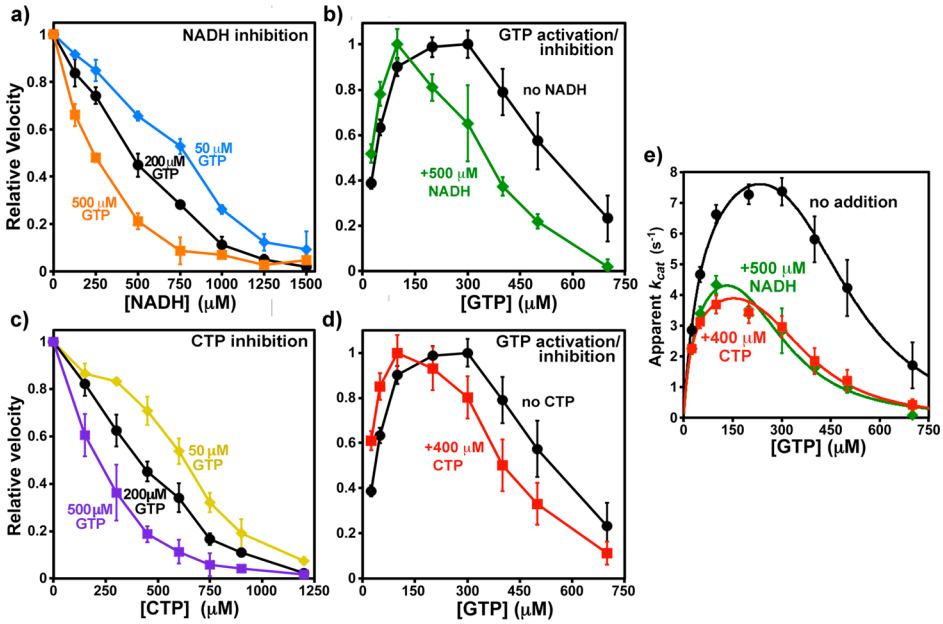

Figure 6. Interactions of CTP or NADH with GTP. Apparent EC_{50} and IC_{50} values are given in Table 3. (a) Relative CTP synthesis velocities with 0−1500 μM NADH in the presence of GTP at 50 μM (blue diamonds), 200 μM (black circles), and 500 μM (orange squares). Error bars indicate the standard deviation for three experiments after normalizing to V_0 equal to one. The V_0 values were 0.64 ± 0.01, 1.21 ± 0.05, and 0.70 ± 0.04 μM s^{-1}, respectively. (b) Relative velocities as a function of 25−700 μM GTP in the absence (black circles) or presence (green squares) of 500 μM NADH. Error bars indicate the standard deviation for four experiments after averaging and then normalizing to V_{max} equal to one. The V_{max} values were 1.47 ± 0.09 and 0.86 ± 0.06 μM s^{-1}, respectively. (c) Relative velocities with 0−1200 μM CTP in the presence of GTP at 50 μM (yellow diamonds), 200 μM (black circles), and 500 μM (purple squares). Error bars indicate the standard deviation for three experiments after normalizing to V_0 equal to one. The V_0 values were 0.65 ± 0.01, 1.16 ± 0.10, and 0.77 ± 0.09 μM s^{-1}, respectively. (d) Relative velocities as a function of 25−700 μM GTP in the absence (black circles) or presence (green squares) of 500 μM NADH. Error bars indicate the standard deviation for four experiments after averaging and then normalizing to V_{max} equal to one. The V_{max} values were 1.47 ± 0.09 and 0.74 ± 0.06 μM s^{-1}, respectively. (e) Fit of GTP titration data to a two-site inhibition model[10] (see Materials and Methods). Unnormalized k_{cat} values with data from experiments with no inhibitor (black circles), 500 μM NADH (green diamonds), or 400 μM CTP (red squares) are shown (see Table 3), along with curves, calculated from the following parameters fit to the averaged data: (i) uninhibited (black circles), k_{act} = 10.0 s^{-1}, K_A = 57 μM, K_i = 301 μM, and n_{inh} = 4.8 (R^2 = 0.993); (ii) NADH inhibited (green diamonds) k_{act} = 6.0 s^{-1}, K_A = 39 μM, K_i = 175 μM, and n_{inh} = 4.1 (R^2 = 0.966); (iii) CTP inhibited (red squares) k_{act} = 4.8 s^{-1}, K_A = 27 μM, K_i = 202 μM, and n_{inh} = 4.5 (R^2 = 0.962).

binds even less tightly than NAD^+ and $NADP^+$ suggesting that the ribo-dinucleotide moiety contributes significantly to their binding. The ADP portion is only a moderate contributor, with ADP inhibiting less well than even 1MeN.

Where are the nicotinamide binding sites? NAD^+ and 1MDHN enhance *Ec*CTPS inhibition by CTP similarly to NADH, supporting the idea that NADH, NAD^+, and 1MDHN induce similar changes in *Ec*CTPS structure, likely by binding to the same site. While the most obvious candidate is the ATP binding site, lack of comparable inhibition by ADP, unchanged v vs [ATP] behavior in the presence of NAD^+ and NADH, and ATP-insensitive NADH dose−response all argue against this idea. The UTP site is also ruled out since NADH inhibition is noncompetitive with UTP and subsaturating UTP does not alter the NADH dose−response.

Another obvious candidate is the GTP inhibitory site. Indeed, NADH inhibition resembles that of guanosine and other purines.[44,53] Like guanosine, NADH inhibits ammonia-dependent synthesis (Figure S6) and similarly shifts both GTP activation and inhibition curves[10,44] (Figure 6e, compare to Figure 4 in ref 44). Potentiation of GTP dual effects is diagnostic for mutual and nonexclusive binding in non-cooperative systems. Although an explicit model is difficult to construct, apparent cooperative binding of NADH and GTP could be exerted allosterically through binding to the same sites on different subunits. A complication is that the locations of the GTP activation and inhibition sites and whether they are distinct are unknown. Although structural comparisons with GTP-binding proteins are suggestive,[2] we have been unable to locate the *bona fide* GTP binding site(s) using crystallography. Soaking *Ec*CTPS crystals in 100 mM GTP loads GTP into the ATP site (James Endrizzi and E.B., unpublished data, Figure S7). However, 500 μM GTP does not significantly modify the UTP or ATP $S_{0.5}$ values, arguing against GTP occupying substrate sites in solution.

The apparent synergism between NADH, CTP, and GTP suggest potential coupling between their binding sites. While mild enhancement of inhibitory potency can result simply from coresidency of noninteracting ligands on the same enzyme particle,[54] the more extensively altered dose−response curve shapes and increased potencies provide clear evidence that binding by one molecule exerts positive cooperativity for the binding the others. Interestingly, the effects of GTP at suboptimal (50 μM), optimal (200 μM), and inhibitory (500 μM) concentrations are remarkably similar on both CTP and NADH (compare Figure 6, panels a and c), where the IC_{50} values show a similar proportional dependence on GTP concentration (see Results). In turn, CTP and NADH have very similar effects on GTP concentration dependences (Figure 6b,d,e).

The mutual effects of NADH, CTP, and GTP are most straightforwardly rationalized by all three inhibitors binding

DOI: 10.1021/acs.biochem.6b00383
Biochemistry 2016, 55, 5554−5565

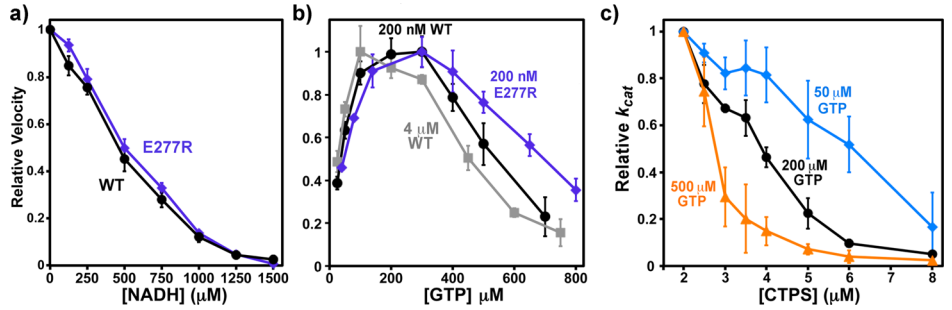

Figure 7. The role of inhibitory filament formation in NADH and GTP inhibition. (a) Relative CTP synthesis velocities of 200 nM WT (black circles) and E277R (see ref 31, indigo diamonds) in the presence of 0−1500 μM NADH normalizing the V_0 equal to one (V_0 (WT) = 1.24 ± 0.05 μM s^{-1}, V_0 (E277R) = 1.07 ± 0.03 μM s^{-1}). Error bars indicate the standard deviation from the average values of three experiments after normalizing V_0 equal to one. The filament blocking mutation E277R does not significantly affect NADH inhibition. (b) Relative velocities of 200 nM WT (black circles), 4 μM WT (gray squares), or 200 nM E277R (indigo diamonds) as a function of 25−800 μM GTP. Error bars indicate the standard deviation from the average of four experiments. For comparison purposes, the maximum velocities of each experiment were normalized to one prior, to averaging. The average V_{max} values were 1.57 ± 0.11 s^{-1} (200 nM WT), 14.0 ± 1.7 s^{-1} (4 μM WT), and 1.60 ± 0.11 μM s^{-1} (200 nM 277R). The E277R mutation reduced both the activating and inhibitory effects of GTP, while high protein concentrations increased them. The EC_{50} and IC_{50} values, respectively, were 38 ± 3 and 540 ± 60 μM (200 nM WT), 27 ± 7 and 455 ± 46 μM (4 μM WT), and 46 ± 6 and 697 ± 4 μM (200 nM E277R). Fitting the data to a two-site activation/inhibition model (fits not shown) yielded the following parameters: for 200 nM WT, k_{act} = 10.7 s^{-1}, K_A = 58 μM, K_i = 301 μM, and n_{inh} = 4.7 (R^2 = 0.993); for 4 μM WT, k_{act} = 4.7 s^{-1}, K_A = 41 μM, K_i = 221 μM, and n_{inh} = 4.1 (R^2 = 0.984); and 200 nM E277R, k_{act} = 10.7 s^{-1}, K_A = 90 μM, K_i = 342 μM, and n_{inh} = 3.8 (R^2 = 0.996). (c) Relative k_{cat} values from at 2−8 μM final *Ec*CTPS in the presence of 50 μM (blue diamonds), 200 μM (black circles), and 500 μM (orange triangles) GTP. Reactions were performed as previously described[31] with annealing carried out at 40 μM *Ec*CTPS. Error bars indicate the standard deviation from the average k_{cat} of three experiments, after normalizing the maximum k_{cat} of each to one. GTP enhances protein-dependent inhibition. The apparent k_{cat} values at 2 μM *Ec*CTPS are 2.9 s^{-1}(50 μM), 5.0 ± 0.1 s^{-1}(200 μM), and 2.7 ± 1.0 s^{-1}(500 μM). The enzyme concentrations for 50% autoinhibition are 6.1 μM (50 μM), 3.9 μM (200 μM), and 2.8 μM (500 μM).

preferentially to the same inhibited enzyme conformation (Figure 1). This conformation is likely accessed by the free enzyme since none of the effectors seem to require the others in order to inhibit. In aggregate, the data implicate separate binding sites for the three inhibitors: lack of CTP site binding by GTP, inability of GTP and NADH to promote filament formation, and CTP and NADH enhancement of both GTP activation and inhibition provide some evidence for "synergy" that is nonexclusive, cooperative binding.[54] However, the complexity and cooperativity of the individual binding isotherms (see next paragraph) make it challenging to distinguish between true synergy, which by definition excludes synergists from binding to the same site even on different subunits,[54] and cooperative additivity (see above) using the data at hand. Practically, this would require extensive analysis of second inhibitor effects at multiple degrees of inhibition by the first, which is beyond the scope of this work.

*Ec*CTPS exhibits uncommon inhibitor dose−responses, hinting at an unusual regulatory strategy and complex patterns of interactions between binding sites. Unlike more typical hyperbolic or sigmoidal responses to ligands, CTP, nicotinamide, and GTP inhibition curves were very linear, were not fit well by typical logit binding models, and yielded nonlinear Hill plots. Although much has been written concerning the deficiencies of Hill plots,[40,55,56] they can be useful for phenomenological characterization, such as in our velocity titrations with UTP and ATP (Table 1). Hill plot curvature can result when there is not a smooth change in binding interactions when successive ligands are bound, that is, uneven cooperativity.[40] Although testing explicit models for ligand binding site−site interactions within *Ec*CTPS tetramers is beyond the resolution of our data, we applied the sequential interaction model of Koshland and co-workers to gain more insight into the unusual dose−response behavior.[40] This model treats all four sites as spatially equivalent and is specified by four independent equilibrium dissociation constants that represent transitions between species with different numbers of bound ligands (see Materials and Methods and Figure 4a).

While low data/parameter ratios precluded convergent solutions in the sequential binding model, the four dissociation constants for CTP, NADH, NADPH, and 1MDHN inhibitions at activating amounts of GTP (50 or 200 μM, Figures 4, 5a,b, and 6a,c) displayed similar trends. Dissociation constant ratios, which indicate cooperativities for each successive binding step, exhibited a consistent but uneven pattern. Binding the second ligand was anticooperative, binding the third was somewhat easier, and binding the final one is essentially concerted with the third ($K_2/K_1 \approx$ 4−40, $K_3/K_2 \approx$ 0.2−0.8, and $K_4/K_3 \approx 10^{-2}$−10^{-5}). When two ligands were present, as for dose−responses of CTP inhibition with NADH, 1MDHN, NAD^+, or GTP (Figures 5b and 6c, Table 3) and NADH inhibition with CTP or GTP (Figures 5a and 6a), the ratios shifted so that the third binding step became highly anticooperative ($K_2/K_1 \approx$ 0.4−0.8, $K_3/K_2 \approx$ 40−250, and $K_4/K_3 \approx 10^{-4}$−10^{-5}). These results suggest that to attain a nearly linear dose−response, *Ec*CTPS has evolved a complex pattern of intersubunit interactions, precluding straightforward and detailed mechanistic explanations for apparent inhibitor synergy and binding cooperativity. Nonetheless, the similar dissociation constant ratio patterns for both inhibitors alone or in the presence of another inhibitor strongly support the idea that all interact with the same conformation of the enzyme and induce similar functional and structural changes.

The recently described CTP-inhibited *Ec*CTPS filaments[31] might have provided an intriguing global explanation for apparent synergism: that the inhibited filaments preferentially bind not only CTP but also NADH and GTP. GTP is a less effective inhibitor of E277R, while increased protein concentration, which favors filament formation, enhances GTP inhibition (Figure 7b). Protein-dependent inhibition is

DOI: 10.1021/acs.biochem.6b00383
Biochemistry 2016, 55, 5554−5565

potentiated by increasing GTP (Figure 7c). GTP behavior mirrors that of CTP[31] and suggests that it also preferentially binds the filament. However, GTP has not been observed in high-resolution cryoEM reconstructions of *Ec*CTPS filaments (Justin Kollman, personal communication). In contrast to GTP, NADH inhibition is not affected by the filament-disrupting E277R mutation (Figure 7a) indicating it does not bind preferentially to the filament.

The minimal scheme for *Ec*CTPS regulation is depicted in Figure 1. Active or free enzymes are sequestered from the CTP synthesis pathway by inhibitor binding. The inhibited tetramer is in equilibrium with the inhibited filament. CTP and GTP preferentially bind the filament over the inhibited tetramer, while nicotinamides bind the inhibited tetramer preferentially or equally to the filament and do not significantly affect this conformational equilibrium.

Our experiments uncovered previously undocumented inhibitory interactions between CTP and GTP. This cooperation provides a further mechanism by which *Ec*CTPS can fine-tune its responses to the outputs of both the GTP and CTP synthesis pathways. In human cells, the key enzyme in GTP synthesis, IMP dehydrogenase, colocalizes with CTPS1, implying that the intracellular regulatory balance between these two nucleotides is fundamentally important.[57]

What is the physiological relevance of *Ec*CTPS nicotinamide inhibition? It might be advantageous to minimize CTPS activity under conditions where CTP, GTP, or NADH/NADPH accumulate, that is, high anabolite levels and low energy and biosynthesis expenditures. However, uncertainties in *free* intracellular concentrations and the complex network of interactions between inhibitors make it difficult to assess the contribution of nicotinamide levels and redox state to *Ec*CTPS output *in vivo*. The inhibitory concentrations determined here *in vitro* are high compared to some previous estimates of absolute intracellular log-phase concentrations.[4,5] However, such measurements are variable and their accuracy is difficult to assess. A recent estimate for total (free and bound) metabolites in glucose-grown, log phase *E. coli* for NADH, NADPH, CTP, and GTP are 83 μM, 120 μM, 2 mM, and 6 mM, respectively.[3] Using respiratory substrates, glycerol and acetate, the average concentrations of NADH and NADPH are even higher (130 μM and 290 μM, respectively), ranging up to 850 μM and 1.7 mM (Supplementary Table 3 from ref 3). These nicotinamide levels in conjunction with saturating concentrations of CTP, GTP or both, may exert significant influence on *Ec*CTPS activity. The higher intracellular NADPH concentrations over NADH could indicate that the phosphorylated form may be the primary effector. Further, while reduced cofactors are more potent inhibitors, we should take care in understating the impact of weaker inhibition by oxidized cofactor. Total NAD^+ cellular concentrations are high in glucose, glycerol, or acetate grown cells (average 2.6 mM, 4.1 mM, and 2.4 mM, respectively, ranging 1.3−13 mM), well within the range expected to effect significant inhibition. On the other hand, $NADP^+$ concentrations are very low (2 μM), much lower than its IC_{50}.

We described inhibition of *Ec*CTPS by redox cofactors that hints of crosstalk between the cellular redox state and pyrimidine biosynthesis. This work further contributes to the emerging view of CTPSs as a regulatory node, subject to a diverse set of inputs that influence complex conformational equilibria in order to precisely balance intracellular nucleotide levels, much like the regulation of nitrogen metabolism by glutamine synthetases.

■ ASSOCIATED CONTENT

Supporting Information

The Supporting Information is available free of charge on the ACS Publications website at DOI: 10.1021/acs.biochem.6b00383.

Dependence of *Ec*CTPS activity on NaCl concentration, time course of *Ec*CTPS activity with preincubation at 21 °C, representative kinetic data for UTP and ATP concentration dependence of *Ec*CTPS velocity and apparent k_{cat}, independence of NADH inhibition on enzyme activity, independence of NADH inhibition on ATP, UTP and glutamine concentrations, NADH inhibits ammonia-dependent CTP synthesis, high GTP binds to the ATP site in *Ec*CTPS crystals, and small increase in *Ec*CTPS specific activity at concentrations greater than 2 μM in 21 °C preincubation step (PDF)

■ AUTHOR INFORMATION

Corresponding Author

*E-mail: epbaldwin@ucdavis.edu.

Funding

This work was funded in part by NIH Grants R01GM63109 and R01GM97073 (E.P.B), as well as 5RO1GM107384 (Z.G), the Human Frontier Science Program (Z.G. and J.K.) and the Department of Molecular and Cellular Biology at UC Davis (E.B.).

Notes

The authors declare no competing financial interest.

■ ACKNOWLEDGMENTS

The authors thank Chris Fraser and Irwin Segel (U.C. Davis) for helpful discussions.

■ ABBREVIATIONS

*Ec*CTPS, *Escherichia coli* CTP synthetase; ATP, adenosine 5′-triphosphate; ADP, adenosine 5′-diphosphate; UTP, uridine-5′-triphosphate; CTP, cytidine-5′-triphosphate; GTP, guanosine-5′-triphosphate; NADH, 1,4 dihydronicotinamide adenine dinucleotide (reduced); NAD^+, nicotinamide adenine dinucleotide (oxidized); NADPH, 1,4 dihydronicotinamide adenine dinucleotide 2′-phosphate (reduced); $NADP^+$, nicotinamide adenine dinucleotide 2′-phosphate (oxidized); 1MDHN, 1-methyl 1,4-dihydronicotinamide; 1MeN, 1-methyl nicotinamide; IPTG, isopropylthiogalactoside; EDTA, ethylene diamine tetraacetic acid; NTA, nitrilo-triacetic acid; V_{max}, maximum enzyme velocity under given conditions; V_0, uninhibited enzyme velocity; k_{cat}, apparent rate constant for the enzyme catalyzed reaction (V/[E]); $S_{0.5}$, substrate concentration required to achieve one-half V_{max}; IC_{50}, inhibitor concentration that reduces enzyme velocity to one-half V_{max}; EC_{50}, activator concentration required to achieve one-half V_{max}; n_H, Hill number

■ REFERENCES

(1) Lieberman, I. (1956) Enzymatic amination of uridine triphosphate to cytidine triphosphate. *J. Biol. Chem.* 222, 765−775.

(2) Endrizzi, J. A., Kim, H., Anderson, P. M., and Baldwin, E. P. (2004) Crystal structure of Escherichia coli cytidine triphosphate synthetase, a nucleotide-regulated glutamine amidotransferase/ATP-

DOI: 10.1021/acs.biochem.6b00383
Biochemistry 2016, 55, 5554−5565

dependent amidoligase fusion protein and homologue of anticancer and antiparasitic drug targets. *Biochemistry 43*, 6447−6463.
(3) Bennett, B. D., Kimball, E. H., Gao, M., Osterhout, R., Van Dien, S. J., and Rabinowitz, J. D. (2009) Absolute metabolite concentrations and implied enzyme active site occupancy in Escherichia coli. *Nat. Chem. Biol. 5*, 593−599.
(4) Buckstein, M. H., He, J., and Rubin, H. (2008) Characterization of nucleotide pools as a function of physiological state in Escherichia coli. *J. Bacteriol. 190*, 718−726.
(5) Traut, T. W. (1994) Physiological concentrations of purines and pyrimidines. *Mol. Cell. Biochem. 140*, 1−22.
(6) Chang, Y. F., and Carman, G. M. (2008) CTP synthetase and its role in phospholipid synthesis in the yeast Saccharomyces cerevisiae. *Prog. Lipid Res. 47*, 333−339.
(7) Goto, M., Omi, R., Nakagawa, N., Miyahara, I., and Hirotsu, K. (2004) Crystal structures of CTP synthetase reveal ATP, UTP, and glutamine binding sites. *Structure 12*, 1413−1423.
(8) Higgins, M. J., Graves, P. R., and Graves, L. M. (2007) Regulation of human cytidine triphosphate synthetase 1 by glycogen synthase kinase 3. *J. Biol. Chem. 282*, 29493−29503.
(9) Kassel, K. M., Au, D. R., Higgins, M. J., Hines, M., and Graves, L. M. (2010) Regulation of human cytidine triphosphate synthetase 2 by phosphorylation. *J. Biol. Chem. 285*, 33727−33736.
(10) MacDonnell, J. E., Lunn, F. A., and Bearne, S. L. (2004) Inhibition of E. coli CTP synthase by the "positive" allosteric effector GTP. *Biochim. Biophys. Acta, Proteins Proteomics 1699*, 213−220.
(11) Mori, G., Chiarelli, L. R., Esposito, M., Makarov, V., Bellinzoni, M., Hartkoorn, R. C., Degiacomi, G., Boldrin, F., Ekins, S., de Jesus Lopes Ribeiro, A. L., Marino, L. B., Centarova, I., Svetlikova, Z., Blasko, J., Kazakova, E., Lepioshkin, A., Barilone, N., Zanoni, G., Porta, A., Fondi, M., Fani, R., Baulard, A. R., Mikusova, K., Alzari, P. M., Manganelli, R., de Carvalho, L. P., Riccardi, G., Cole, S. T., and Pasca, M. R. (2015) Thiophenecarboxamide Derivatives Activated by EthA Kill Mycobacterium tuberculosis by Inhibiting the CTP Synthetase PyrG. *Chem. Biol. (Oxford, U. K.) 22*, 917−927.
(12) Hofer, A., Steverding, D., Chabes, A., Brun, R., and Thelander, L. (2001) Trypanosoma brucei CTP synthetase: a target for the treatment of African sleeping sickness. *Proc. Natl. Acad. Sci. U. S. A. 98*, 6412−6416.
(13) Williams, J. C., Kizaki, H., Weber, G., and Morris, H. P. (1978) Increased CTP synthetase activity in cancer cells. *Nature 271*, 71−73.
(14) Kursula, P., Flodin, S., Ehn, M., Hammarstrom, M., Schuler, H., Nordlund, P., and Stenmark, P. (2006) Structure of the synthetase domain of human CTP synthetase, a target for anticancer therapy. *Acta Crystallogr., Sect. F: Struct. Biol. Cryst. Commun. 62*, 613−617.
(15) Lauritsen, I., Willemoes, M., Jensen, K. F., Johansson, E., and Harris, P. (2011) Structure of the dimeric form of CTP synthase from Sulfolobus solfataricus. *Acta Crystallogr., Sect. F: Struct. Biol. Cryst. Commun. 67*, 201−208.
(16) Lewis, D. A., and Villafranca, J. J. (1989) Investigation of the mechanism of CTP synthetase using rapid quench and isotope partitioning methods. *Biochemistry 28*, 8454−8459.
(17) von der Saal, W., Anderson, P. M., and Villafranca, J. J. (1985) Mechanistic investigations of Escherichia coli cytidine-5′-triphosphate synthetase. Detection of an intermediate by positional isotope exchange experiments. *J. Biol. Chem. 260*, 14993−14997.
(18) Long, C. W., Levitzki, A., and Koshland, D. E., Jr. (1970) The subunit structure and subunit interactions of cytidine triphosphate synthetase. *J. Biol. Chem. 245*, 80−87.
(19) Anderson, P. M. (1983) CTP synthetase from Escherichia coli: an improved purification procedure and characterization of hysteretic and enzyme concentration effects on kinetic properties. *Biochemistry 22*, 3285−3292.
(20) Thomas, P. E., Lamb, B. J., and Chu, E. H. (1988) Purification of cytidine-triphosphate synthetase from rat liver, and demonstration of monomer, dimer and tetramer. *Biochim. Biophys. Acta, Protein Struct. Mol. Enzymol. 953*, 334−344.
(21) Pappas, A., Yang, W. L., Park, T. S., and Carman, G. M. (1998) Nucleotide-dependent tetramerization of CTP synthetase from Saccharomyces cerevisiae. *J. Biol. Chem. 273*, 15954−15960.
(22) Lunn, F. A., Macleod, T. J., and Bearne, S. L. (2008) Mutational analysis of conserved glycine residues 142, 143 and 146 reveals Gly(142) is critical for tetramerization of CTP synthase from Escherichia coli. *Biochem. J. 412*, 113−121.
(23) Endrizzi, J. A., Kim, H., Anderson, P. M., and Baldwin, E. P. (2005) Mechanisms of product feedback regulation and drug resistance in cytidine triphosphate synthetases from the structure of a CTP-inhibited complex. *Biochemistry 44*, 13491−13499.
(24) Choi, M. G., Park, T. S., and Carman, G. M. (2003) Phosphorylation of Saccharomyces cerevisiae CTP synthetase at Ser424 by protein kinases A and C regulates phosphatidylcholine synthesis by the CDP-choline pathway. *J. Biol. Chem. 278*, 23610−23616.
(25) Han, G. S., Sreenivas, A., Choi, M. G., Chang, Y. F., Martin, S. S., Baldwin, E. P., and Carman, G. M. (2005) Expression of Human CTP synthetase in Saccharomyces cerevisiae reveals phosphorylation by protein kinase A. *J. Biol. Chem. 280*, 38328−38336.
(26) Park, T. S., O'Brien, D. J., and Carman, G. M. (2003) Phosphorylation of CTP synthetase on Ser36, Ser330, Ser354, and Ser454 regulates the levels of CTP and phosphatidylcholine synthesis in Saccharomyces cerevisiae. *J. Biol. Chem. 278*, 20785−20794.
(27) Carcamo, W. C., Satoh, M., Kasahara, H., Terada, N., Hamazaki, T., Chan, J. Y., Yao, B., Tamayo, S., Covini, G., von Muhlen, C. A., and Chan, E. K. (2011) Induction of cytoplasmic rods and rings structures by inhibition of the CTP and GTP synthetic pathway in mammalian cells. *PLoS One 6*, e29690.
(28) Ingerson-Mahar, M., Briegel, A., Werner, J. N., Jensen, G. J., and Gitai, Z. (2010) The metabolic enzyme CTP synthase forms cytoskeletal filaments. *Nat. Cell Biol. 12*, 739−746.
(29) Liu, J. L. (2010) Intracellular compartmentation of CTP synthase in Drosophila. *J. Genet. Genomics 37*, 281−296.
(30) Noree, C., Sato, B. K., Broyer, R. M., and Wilhelm, J. E. (2010) Identification of novel filament-forming proteins in Saccharomyces cerevisiae and Drosophila melanogaster. *J. Cell Biol. 190*, 541−551.
(31) Barry, R. M., Bitbol, A. F., Lorestani, A., Charles, E. J., Habrian, C. H., Hansen, J. M., Li, H. J., Baldwin, E. P., Wingreen, N. S., Kollman, J. M., and Gitai, Z. (2014) Large-scale filament formation inhibits the activity of CTP synthetase. *eLife 3*, e03638.
(32) Calise, S. J., Carcamo, W. C., Krueger, C., Yin, J. D., Purich, D. L., and Chan, E. K. (2014) Glutamine deprivation initiates reversible assembly of mammalian rods and rings. *Cell. Mol. Life Sci. 71*, 2963−2973.
(33) Aughey, G. N., Grice, S. J., Shen, Q. J., Xu, Y., Chang, C. C., Azzam, G., Wang, P. Y., Freeman-Mills, L., Pai, L. M., Sung, L. Y., Yan, J., and Liu, J. L. (2014) Nucleotide synthesis is regulated by cytoophidium formation during neurodevelopment and adaptive metabolism. *Biol. Open 3*, 1045−1056.
(34) Noree, C., Monfort, E., Shiau, A. K., and Wilhelm, J. E. (2014) Common regulatory control of CTP synthase enzyme activity and filament formation. *Mol. Biol. Cell 25*, 2282−2290.
(35) Levitzki, A., and Koshland, D. E., Jr. (1972) Ligand-induced dimer-to-tetramer transformation in cytosine triphosphate synthetase. *Biochemistry 11*, 247−253.
(36) Ortiz-Maldonado, M., Gatti, D., Ballou, D. P., and Massey, V. (1999) Structure-function correlations of the reaction of reduced nicotinamide analogues with p-hydroxybenzoate hydroxylase substituted with a series of 8-substituted flavins. *Biochemistry 38*, 16636−16647.
(37) Wang, S. Y. (1968) Photochemistry of N1-methylnicotinamide salts. *Biochemistry 7*, 3740−3744.
(38) Robertson, J. G., and Villafranca, J. J. (1993) Characterization of metal ion activation and inhibition of CTP synthetase. *Biochemistry 32*, 3769−3777.
(39) Long, C. W., and Pardee, A. B. (1967) Cytidine triphosphate synthetase of Escherichia coli B. I. Purification and kinetics. *J. Biol. Chem. 242*, 4715−4721.

DOI: 10.1021/acs.biochem.6b00383
Biochemistry 2016, 55, 5554−5565

(40) Cornish-Bowden, A., and Koshland, D. E., Jr. (1975) Diagnostic uses of the Hill (Logit and Nernst) plots. *J. Mol. Biol. 95*, 201−212.
(41) Levitzki, A., Stallcup, W. B., and Koshland, D. E., Jr. (1971) Half-of-the-sites reactivity and the conformational states of cytidine triphosphate synthetase. *Biochemistry 10*, 3371−3378.
(42) MacLeod, T. J., Lunn, F. A., and Bearne, S. L. (2006) The role of lysine residues 297 and 306 in nucleoside triphosphate regulation of E. coli CTP synthase: inactivation by 2′,3′-dialdehyde ATP and mutational analyses. *Biochim. Biophys. Acta, Proteins Proteomics 1764*, 199−210.
(43) Robertson, J. G. (1995) Determination of subunit dissociation constants in native and inactivated CTP synthetase by sedimentation equilibrium. *Biochemistry 34*, 7533−7541.
(44) Lunn, F. A., MacDonnell, J. E., and Bearne, S. L. (2008) Structural requirements for the activation of Escherichia coli CTP synthase by the allosteric effector GTP are stringent, but requirements for inhibition are lax. *J. Biol. Chem. 283*, 2010−2020.
(45) Gruning, N. M., Lehrach, H., and Ralser, M. (2010) Regulatory crosstalk of the metabolic network. *Trends Biochem. Sci. 35*, 220−227.
(46) Brekasis, D., and Paget, M. S. (2003) A novel sensor of NADH/NAD+ redox poise in Streptomyces coelicolor A3(2). *EMBO J. 22*, 4856−4865.
(47) Ravcheev, D. A., Li, X., Latif, H., Zengler, K., Leyn, S. A., Korostelev, Y. D., Kazakov, A. E., Novichkov, P. S., Osterman, A. L., and Rodionov, D. A. (2012) Transcriptional regulation of central carbon and energy metabolism in bacteria by redox-responsive repressor Rex. *J. Bacteriol. 194*, 1145−1157.
(48) Scheer, M., Grote, A., Chang, A., Schomburg, I., Munaretto, C., Rother, M., Sohngen, C., Stelzer, M., Thiele, J., and Schomburg, D. (2011) BRENDA, the enzyme information system in 2011. *Nucleic Acids Res. 39*, D670−676.
(49) Duckworth, H. W., Anderson, D. H., Bell, A. W., Donald, L. J., Chu, A. L., and Brayer, G. D. (1987) Structural basis for regulation in gram-negative bacterial citrate synthases. *Biochem. Soc. Symp. 54*, 83−92.
(50) Jenkins, J. A., Johnson, L. N., Stuart, D. I., Stura, E. A., Wilson, K. S., Zanotti, G., and Wilkie, D. R. (1981) Phosphorylase: control and activity. *Philos. Trans. R. Soc., B 293*, 23−41.
(51) Runquist, J. A., Narasimhan, C., Wolff, C. E., Koteiche, H. A., and Miziorko, H. M. (1996) Rhodobacter sphaeroides phosphoribulokinase: binary and ternary complexes with nucleotide substrate analogs and effectors. *Biochemistry 35*, 15049−15056.
(52) Devin, A., Nogueira, V., Leverve, X., Guerin, B., and Rigoulet, M. (2001) Allosteric activation of pyruvate kinase via NAD+ in rat liver cells. *Eur. J. Biochem. 268*, 3943−3949.
(53) Roy, A. C., Lunn, F. A., and Bearne, S. L. (2010) Inhibition of CTP synthase from Escherichia coli by xanthines and uric acids. *Bioorg. Med. Chem. Lett. 20*, 141−144.
(54) Breitinger, H.-G. (2012) Drug Synergy − Mechanisms and Methods of Analysis, in *Toxicity and Drug Testing* (Acree, W., Ed.), pp 143−166, InTech, Rijeka, Croatia, DOI: 10.5772/30922.
(55) Bindslev, N. (2008) *Drug-Acceptor Interactions: Modeling Theoretical Tools to Test and Evaluate Experimental Equilibrium Effects*; Co-Action Publishing, Järfälla, Sweden.
(56) Ricard, J., and Cornish-Bowden, A. (1987) Co-operative and allosteric enzymes: 20 years on. *Eur. J. Biochem. 166*, 255−272.
(57) Carcamo, W. C., Calise, S. J., von Muhlen, C. A., Satoh, M., and Chan, E. K. (2014) Molecular cell biology and immunobiology of mammalian rod/ring structures. *Int. Rev. Cell Mol. Biol. 308*, 35−74.
(58) Iyengar, A., and Bearne, S. L. (2002) An assay for cytidine 5(′)-triphosphate synthetase glutaminase activity using high performance liquid chromatography. *Anal. Biochem. 308*, 396−400.

DOI: 10.1021/acs.biochem.6b00383
Biochemistry 2016, 55, 5554−5565

Supporting Information for

Inhibition of *E. coli* CTP synthetase by NADH and other nicotinamides, and their mutual interactions with CTP and GTP

Chris Habrian, Adithi Chandrasekhara, Bita Shahrvini, Brian Hua, Jason Lee, Roger

Jesinghaus, Rachael Barry, Zemer Gitai, Justin Kollman and Enoch P. Baldwin

List of Supporting Figures

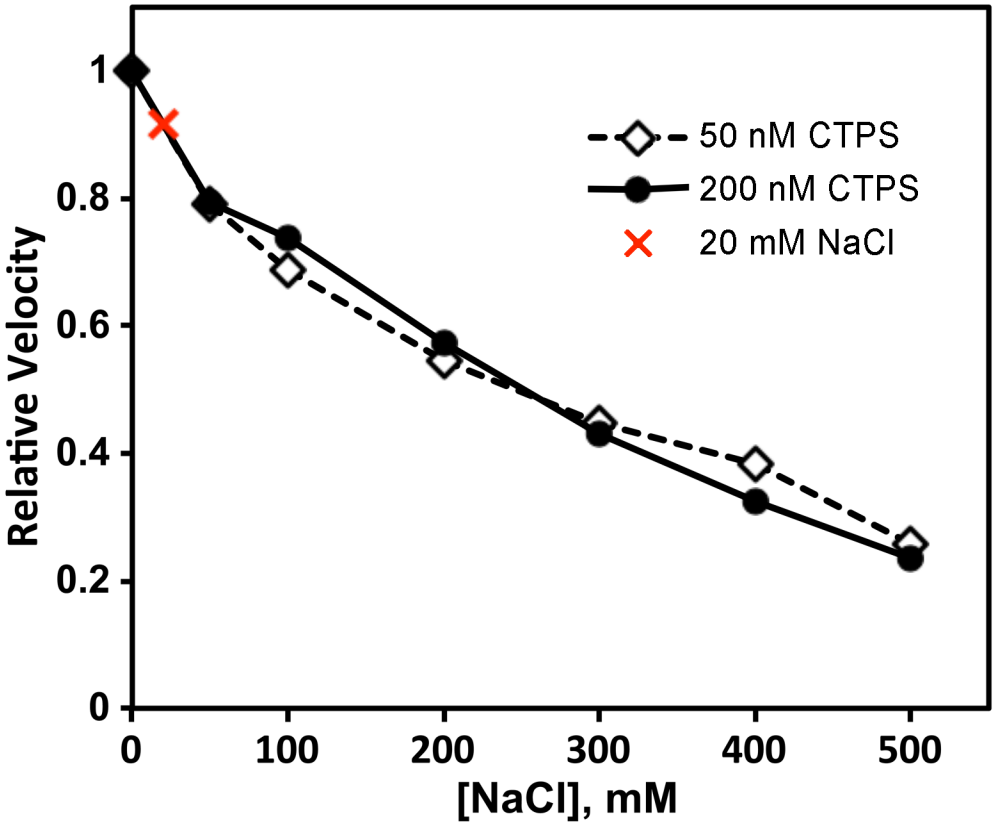

Figure S1. "At 8 uM final EcCTP concentration, the NaCl contribution from enzyme stocks did not exceed 20 mM, which has a negligible effect on rate (data not shown)."

Standard assay conditions were utilized at 50 nM (white diamonds) and 200 nM (black circles) *Ec*CTPS. For preincubation, 0, 50, 100, 200, 300, 400 and 500 mM NaCl (final concentration in assay) was added to the A tubes (See **Materials and Methods**). At 20 mM NaCl, activity was reduced ~8%.

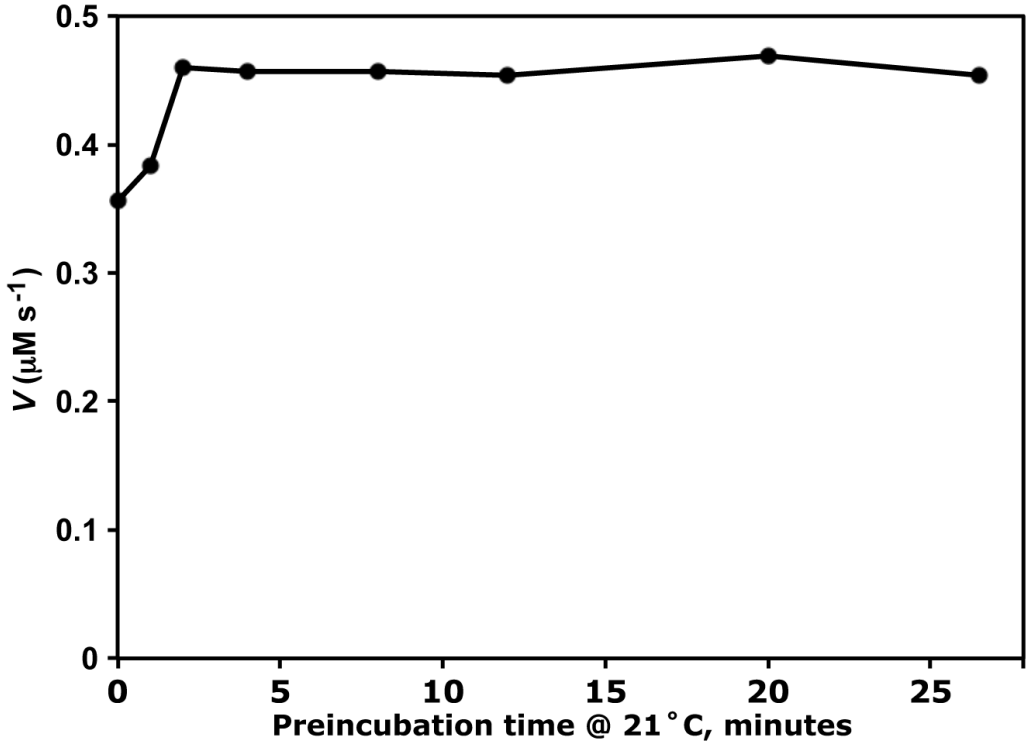

Figure S2. "The annealing procedure, which is aimed at maximizing dimer reassembly, improved assay reproducibility and increased the specific activity by 20-40%" Representative experiment showing the effect of 21˚C preincubation for 0, 1, 2, 4, 8, 12, 20 and 27 minutes at 1 μM CTPS in reaction buffer (60 mM Na-HEPES, 10 mM $MgCl_2$, pH 8.0), followed by mixing with A tubes containing reaction buffer, 150 uM UTP, 1 mM ATP, 0.2 mM GTP (final concentrations) and further incubation at 37˚C. After 90 seconds, 10 mM glutamine was added and the change in A_{291} was measured. In this experiment, activity increased 28%. Increases ranged 20-40%. The experiment also demonstrates that EcCTPS retains its activity for at least 25-30 minutes at 21˚C.

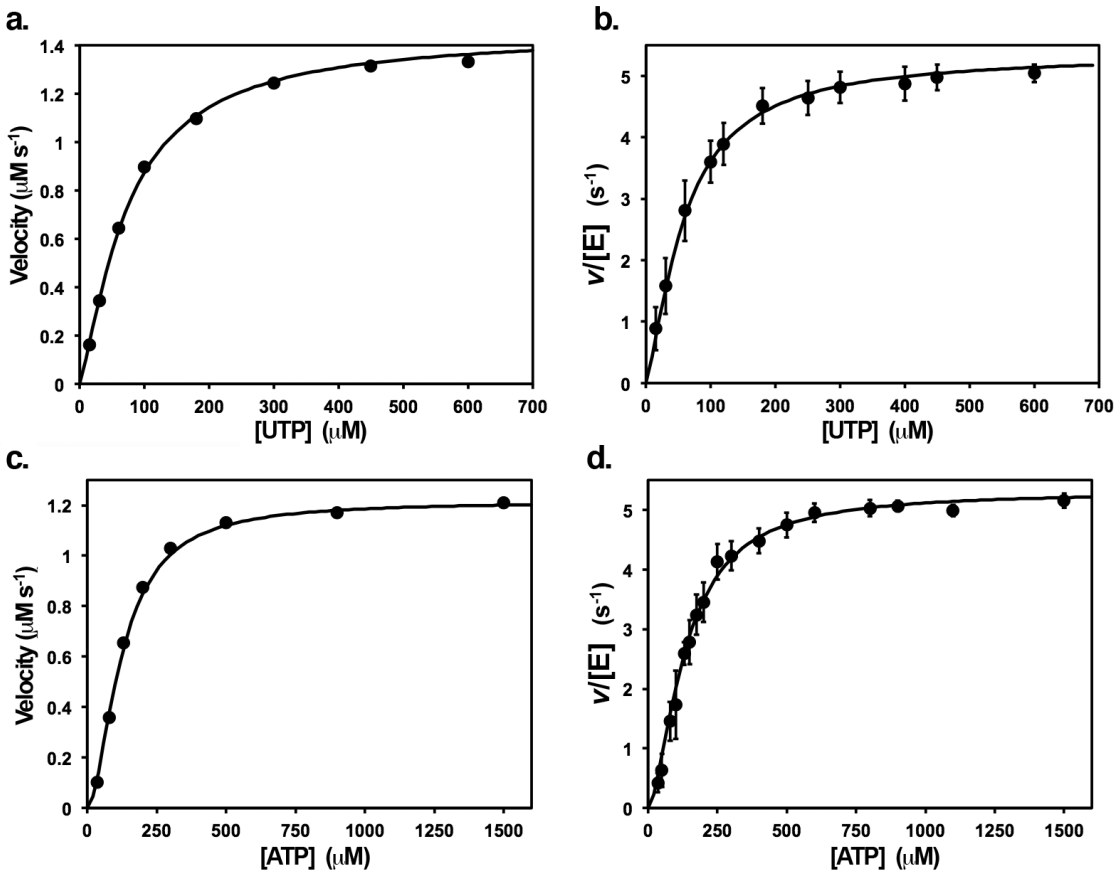

Figure S3. Representative kinetic data for UTP and ATP concentration dependence of *Ec*CTPS velocity and apparent k_{cat}.

Kinetic data were acquired as described in **Materials and Methods**. **(a)** Sample single experiment for UTP dependence at 15, 30, 60 100, 180, 300, 450, and 600 μM UTP, 200 nM *Ec*CTPS, 1.5 mM ATP, 200 μM GTP in 60 mM Na-HEPES, 10 mM $MgCl_2$, 0.5 mM Na-EGTA, pH 8.0. Additional Na^+ ion contributions from nucleotides range from 8 mM (0 μM UTP) to 11 mM (600 μM UTP). The fit curve was calculated using the Hill equation with the following parameters: $S_{0.5}$ = 72 μM, V_{max}= 1.45 μM s^{-1} and n_H = 1.3. **(b)** Merged data from 21 separate experiments titrating 0-600 μM UTP as described in (a) and **Materials and Methods**. Data from different enzyme concentrations were used since the $S_{0.5}$ and n_H values did not differ

significantly from 15-2000 nM enzyme, although apparent k_{cat} values ranged 2.4 – 7.2 s^{-1}. V/[E] values were normalized to the mean for all of the experiments (5.4 ± 1.4 s^{-1}) and then averaged. Each data point represents the mean of normalized data for 5 to 21 individual measurements. The fit line was calculated from averaged parameters for 23 experiments $S_{0.5}$ = 59 μM, V/[E]= 5.35 μM s^{-1} and n_H = 1.4 (R^2 = 0.999, Table 1). The Solver non-linear regression solution for the averaged data was $S_{0.5}$ = 54 μM, V/[E]= 5.27 μM s^{-1} and n_H = 1.33. **(c)** Sample data for the velocity dependence on ATP concentration (35, 80, 130, 200, 300, 500, 900, and 1500 μM ATP, 600 μM UTP, and as in (a)). Additional Na^+ ion contributions varied from 4-11 mM. The fit curve was calculated using the Hill equation: $S_{0.5}$ = 125 μM, V_{max}= 1.22 μM s^{-1} and n_H = 1.8. **(d)** Merged data from 18 separate experiments titrating 0-1500 μM ATP, and [*Ec*CTPS] ranging 50-400 nM, with apparent k_{cat} values ranging 3.7 – 6.6 s^{-1}. V/[E] values for each point were normalized to the mean for all of the experiments (5.3 ± 0.9 s^{-1}) and then averaged (n=3-18). The fit line was calculated from averaged parameters for 18 experiments $S_{0.5}$ = 130 μM, V/[E]= 5.30 μM s^{-1} and n_H = 1.7 (R^2=0.995, Table 1). The Solver non-linear regression solution for the averaged data was $S_{0.5}$ = 134, V/[E]= 5.16 μM s^{-1} and n_H = 1.8.

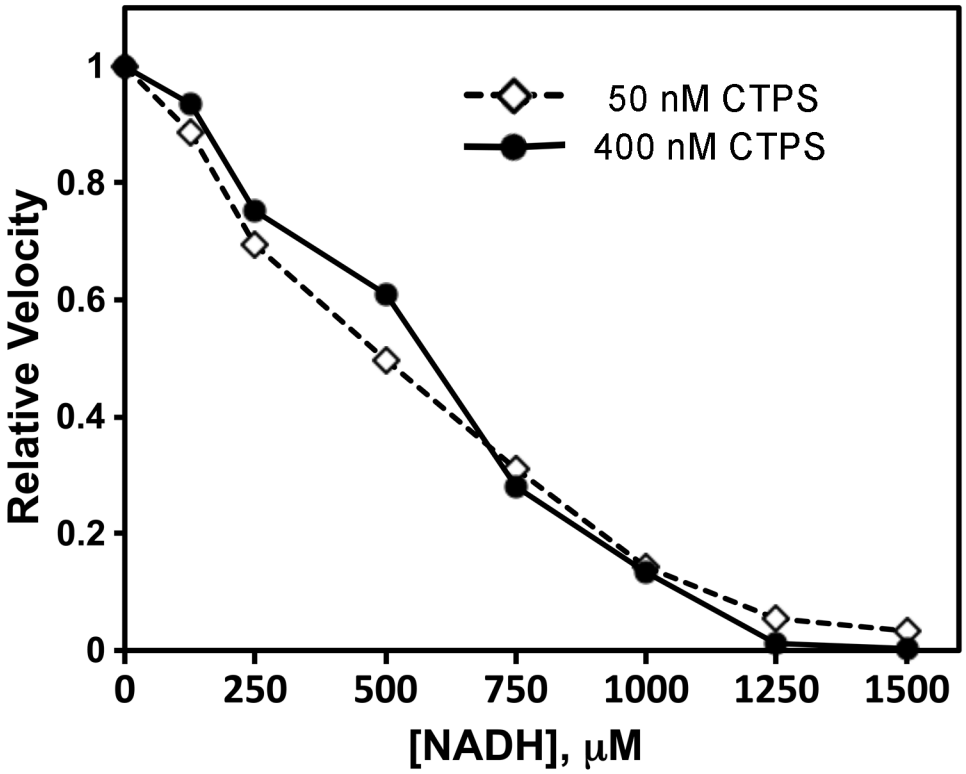

Figure S4. "(NADH) Inhibition potency was independent of enzyme concentration from 50-400 nM."

In a representative experiment, *Ec*CTPS, 50 and 400 nM (final), was assayed under standard conditons in the presence of 0, 100, 250, 500, 750, 1000, 1250 and 1500 μM NADH. Both experiments yielded similar titration curves after normalizing V_o = 1 (V_o values were 0.33 μM s^{-1}(50 nM) and 2.58 μM s^{-1} (200 nM)).

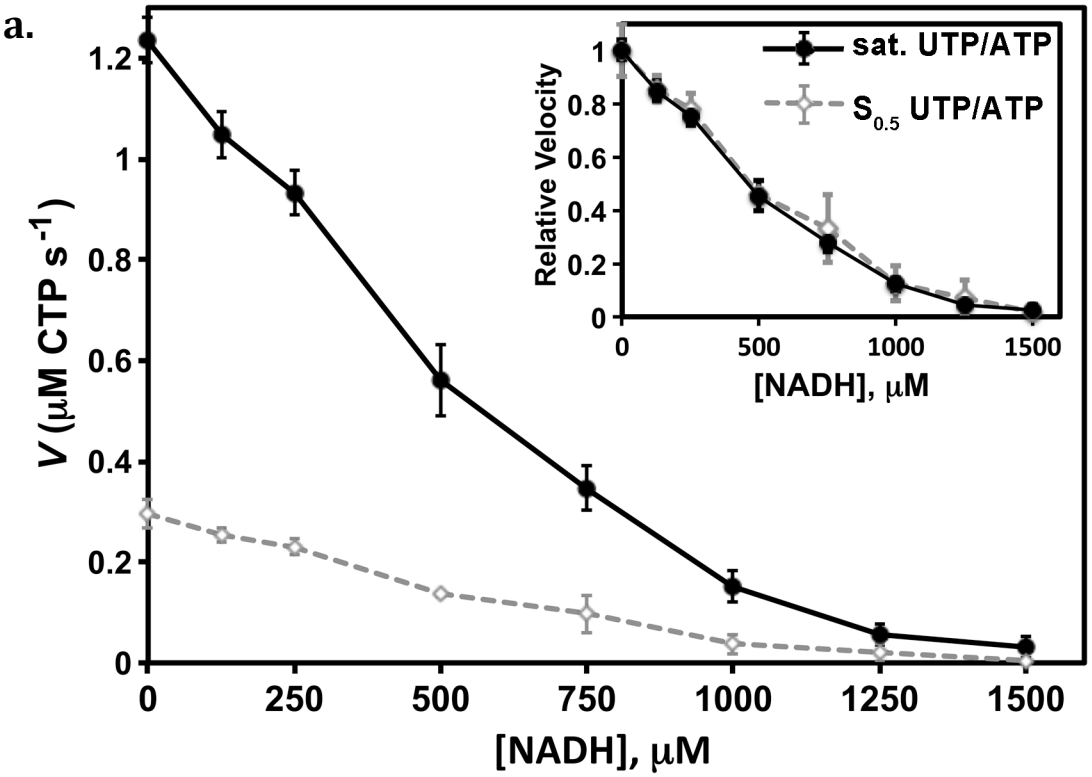
a.
V (μM CTP s-1)
[NADH], μM
sat. UTP/ATP
S0.5 UTP/ATP
Relative Velocity
[NADH], μM

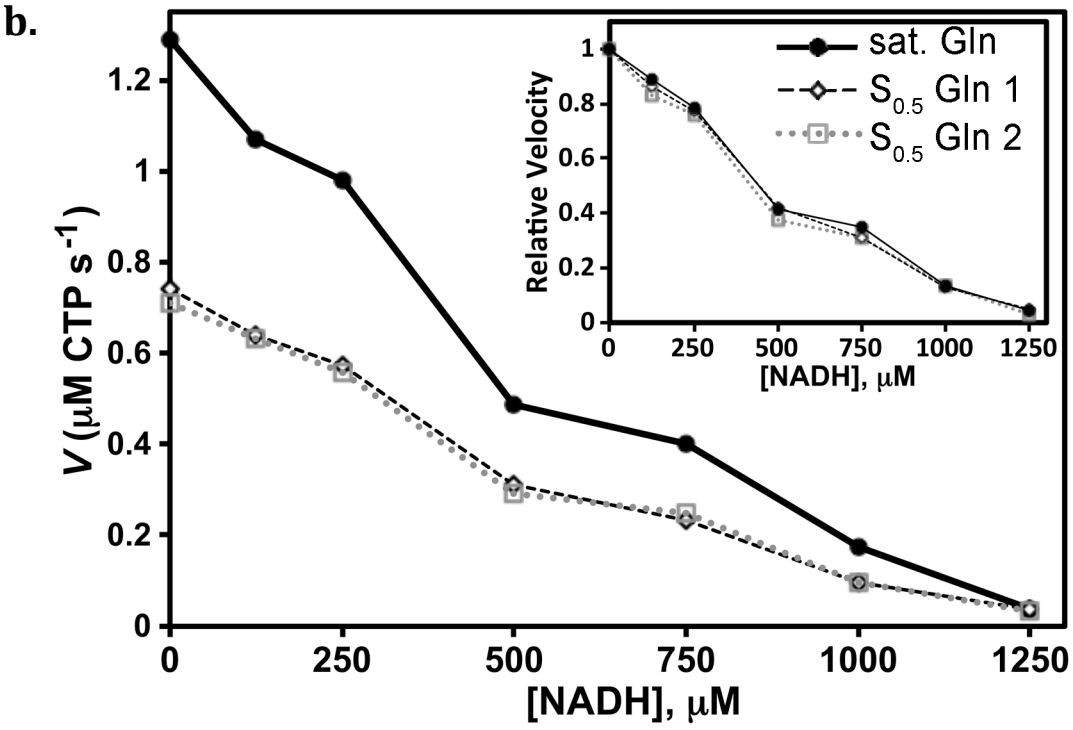
b.
V (μM CTP s-1)
[NADH], μM
sat. Gln
S0.5 Gln 1
S0.5 Gln 2
Relative Velocity
[NADH], μM

Figure S5. "Conversely, when titrated in the presence of ATP, UTP or glutamine substrates at their $S_{0.5}$ values, the NADH dose-response curves were identical to those with saturating substrates (data not shown)."

*Ec*CTPS activity was assessed in the presence of 0-1250 μM NADH, and $S_{0.5}$ or saturating (10x $S_{0.5}$) concentrations of **(a)** both ATP and UTP or **(b)** glutamine. Insets show data normalized to V_o. For (a), the mean values and standard deviations of three experiments are shown. For (b), a representative experiment with one set determined with saturating glutamine and two at $S_{0.5}$ glutamine. For $S_{0.5}$ values, see Table 1. V_o values are (a) 0.30 μM s^{-1}($S_{0.5}$ ATP and UTP) and 1.24 μM s^{-1} (saturating ATP and UTP); and (b) 0.74 μM s^{-1} and 0.71 μM s^{-1} ($S_{0.5}$ glutamine) and 1.29 μM s^{-1} (saturating glutamine).

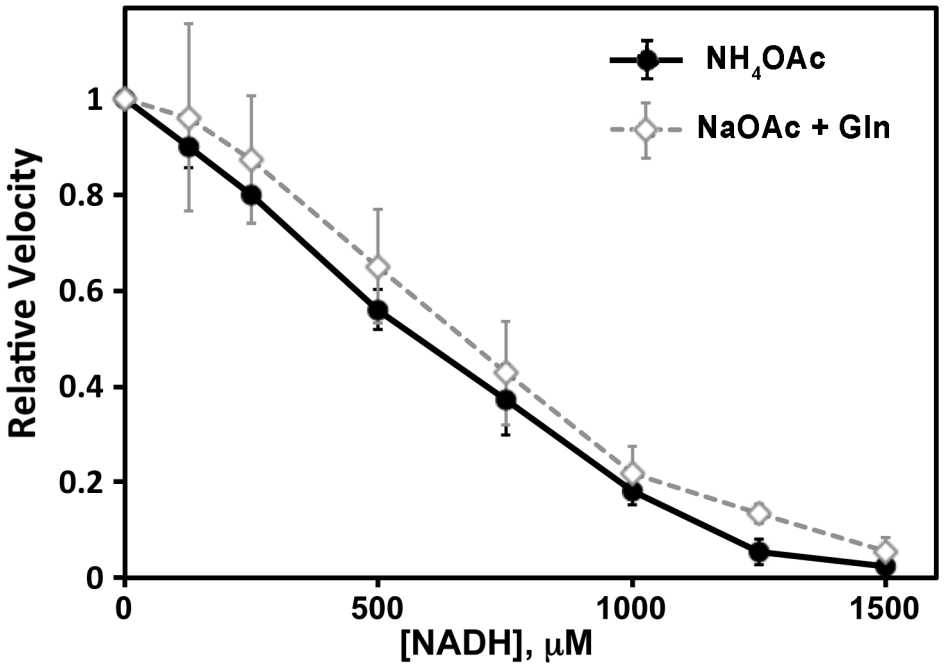

Figure S6. "Like guanosine, NADH inhibited ammonia-dependent synthesis**…**"

*Ec*CTPS activity was assayed using ammonia (black filled circles) or glutamine (grey open diamonds) as a nitrogen source. Reactions were carried out under standard conditions as described in **Materials and Methods**, except that C tubes contained either 1 M ammonium acetate or 100 mM glutamine in 1 M sodium acetate (pH 8.0, 100 mM final acetate). The data were averaged after normalizing V_o values of each experiment to one (n=3). The apparent IC50 values are nearly identical. The differences in ionic strength and composition slightly increased the IC50 values (580±60 mM for NH_4OAc, and 660±130 mM for NaOAc+glutamine) and reduced the apparent k_{cat} values (5.3±0.1 s^{-1} for NH_4OAc, and 3.7±0.3 s^{-1} for NaOAc+glutamine), compared to standard conditions without acetate.

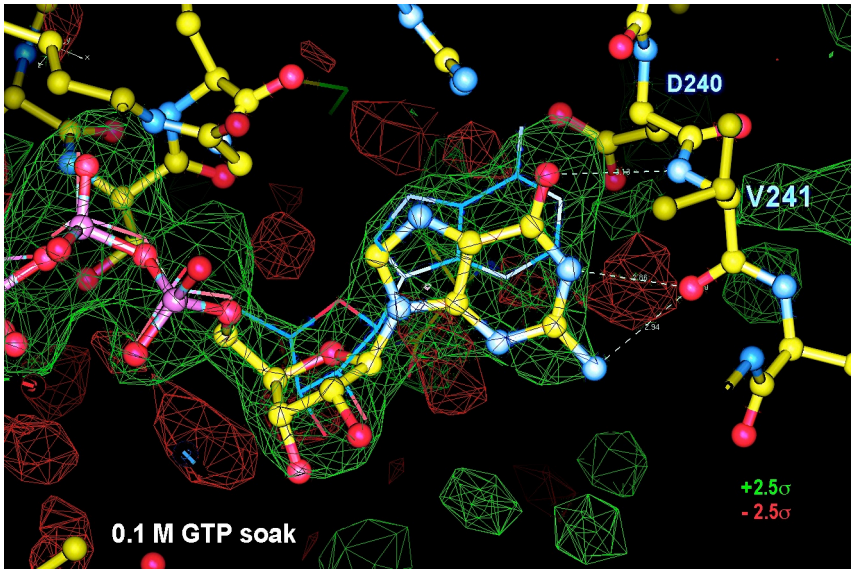

Figure S7. "Soaking *Ec*CTPS crystals in 100 mM GTP loads GTP into the ATP site (James Endrizzi and E.P.B., *unpublished data*). "

Crystals of recombinant His6-tagged EcCTPS, grown from ammonium sulfate as previously described for native CTPS (Endrizzi *et al.*, (2005)), were soaked with 0.1 M GTP for 1 hour at 4˚C before cryprotection with 25% MPD. Data were collected at SSRL Beamline 1-5 (100-2.4-Å resolution, 99.9/3.6 completeness/multiplicity (2.54-2.4 Å; 99.9/3.6), Rmerge=0.088 (2.54-2.4 Å; 0.42)). Refmac 5 maximum likelihood refinement starting with ligand/water-free PDB model 1S1M (R/Rfree = 21.6/25.1) (Endrizzi *et al.*, (2005)), yielded the above difference map (visualized using COOT). The GTP position was derived with 30 cycles of further refinement with GTP (R/Rfree = 20.9/24.2%). Shown for comparison is the ADP pose from PDB model 2AD5 after superposition of residues 1-260. Note the change in H-bonding pattern due to the shift in purine ring positions.

Although GTP binds the ATP site in the crystal, we view this as an artifact since there is no kinetic evidence for competition between ATP and GTP in ATP titration experiments.

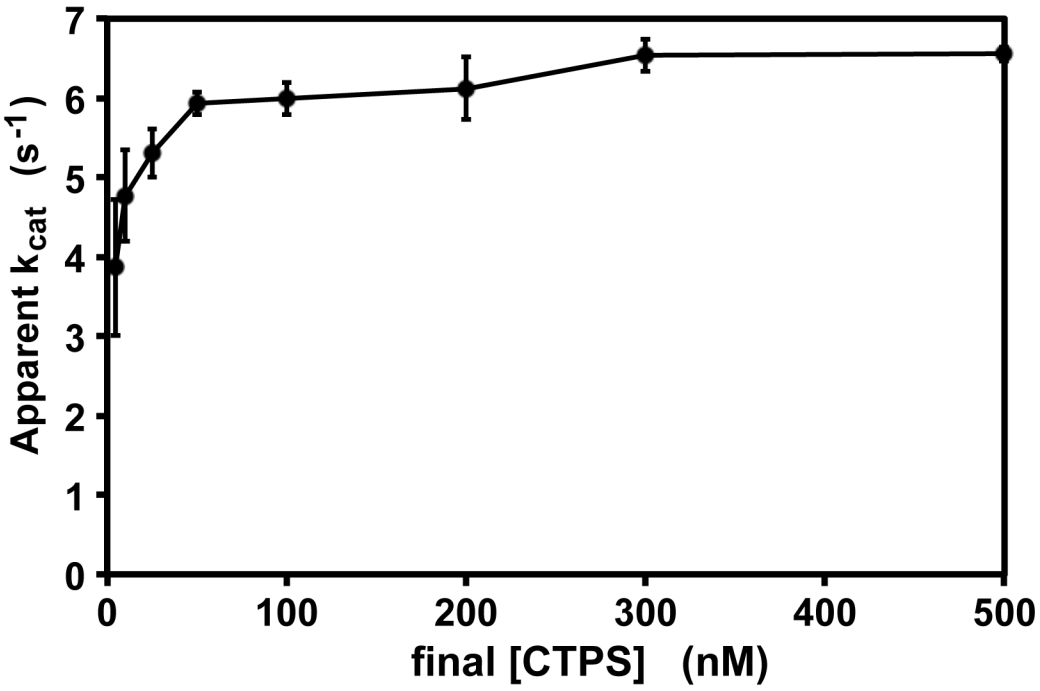

Figure S8. Figure 2 Legend: "Under these conditions, k_{cat} increases approximately 5-9% going from 100-500 nM final *Ec*CTPS (data not shown)."

Assay was performed as described in the Figure 2 legend.